Physics – Uspekhi **60** (11) 1067 – 1086 (2017)

REVIEWS OF TOPICAL PROBLEMS

PACS numbers: 05.60.Gg, 68.37.Ef, 73.40.Gk, **73.63. – b**

IN MEMORY OF LEONID VENIAMINOVICH KELDYSH

Tunneling features in semiconductor nanostructures

P I Arseev, V N Mantsevich, N S Maslova, V I Panov

DOI: https://doi.org/10.3367/UFNe.2017.01.038055

Contents

Abstract. **The most telling scanning tunneling microscopy/spectroscopy (STM/STS) data available on the influence of nonequilibrium tunneling effects and electronic spectra reconstruction are reviewed and theoretically explained by self-consistently accounting for nonequilibrium electron distribution and the change (due to the tunneling current) in the electron density of states near the tunneling junction. The paper discusses the basic ideas of the self-consistent tunneling theory, which forms the basis for experimental research and which allows many effects observed in STM/STS experiments to be explained and new phenomena to be predicted.**

Keywords: tunneling, scanning tunneling microscopy/spectroscopy, localized states, Keldysh diagram technique, nonequilibrium processes, interparticle interaction

P I Arseev, Lebedev Physical Institute, Russian Academy of Sciences, Leninskii prosp. 53, 119991 Moscow, Russian Federation;
National Research University 'Higher School of Economics', ul. Myasnitskaya 20, 101000 Moscow, Russian Federation
E-mail: ars@lpi.ru
V N Mantsevich, N S Maslova, V I Panov
Lomonosov Moscow State University, Leninskie gory 1, 119991 Moscow, Russian Federation
E-mail: vmantsev@gmail.com, nsmaslova@gmail.com, panov@spmlab.phys.msu.ru

Received 12 December 2016
Uspekhi Fizicheskikh Nauk **187** (11) 1147 – 1168 (2017)
DOI: https://doi.org/10.3367/UFNr.2017.01.038055
Translated by K B Alkalaev; edited by A Radzig

We dedicate this paper to L V Keldysh, who initiated experimental work on scanning tunneling microscopy/spectroscopy at Moscow State University and created the nonequilibrium diagram technique that allowed formulating a consistent theoretical description of tunneling processes.

1. Introduction

The building of a scanning tunneling microscope (STM) allowed the use of the tunnel effect to investigate surface electronic and atomic structures and surface nanostructures. Moreover, it became possible to study local tunneling phenomena on the atomic scale. Already in the first experiments on reconstructed silicon surface 'Si(111)-(7×7)' [1], it was shown that STM allows us to obtain images of surface atomic structures to within the charge state of a separate atom. Over the years of application and development, scanning tunneling microscopy and spectroscopy (STM/STS) became one of the most effective methods to study local tunneling phenomena and properties of the surface structures with atomic resolution. As a result, there is a potential to consider a spatial distribution of impurity states, as well as identify an atomic impurity or a defect of atomic size by means of the peculiarities in tunneling conductance spectrum and its STM image [2–7]. At the same time, those tunneling peculiarities in the STM contacts whose characteristic size is comparable to the interatomic distance often lead to a strong distortion of the unperturbed density of states in a system under consideration. In equilibrium conditions, this can stem from localized states in the contact area (e.g., those associated with a periodic structure break at the end of the STM tip, impurity atoms or defects, etc.) and their interactions with continuous spectrum states in the contact leads.

In STM/STS studies, even separate localized states can have a significant impact on the resulting STM images and

tunneling conductance spectra. This is in contrast to experiments on macroscopic tunneling contacts, where the contribution from the low-density localized states to the tunneling current is negligibly small. By reducing the size of a system, the relaxation time for tunneling electrons becomes comparable to characteristic tunneling times. Thus, a particle distribution becomes essentially nonequilibrium. In the presence of interparticle interaction, the distribution also changes the density of states. For these reasons, the study of the properties of surface nanosystems and local tunneling effects by STM/STS requires considering various relaxation processes (scattering on impurities and inhomogeneities at the sample edge, electron–phonon interaction, etc). As a consequence, it is often hard to interpret the results of experimental investigation of local tunneling conductance and, in some cases, of the analysis of STM images of the investigated nanostructures.

Therefore, in order to describe results of STM/STS measurements appropriately, it is necessary to modify the theoretical approaches applied to the analysis of tunneling processes. We found out that the inference about always existing correspondence between the tunneling current and the initial density of states in the material (electronic system) is generally incorrect. As a result of the interaction of the sample with the nearby STM tip, the initial density of states is distorted so that new bound states arise. The states play a pivotal role in studying impurities, atomic defects, dielectric materials (thin films), surface charge-density waves (CDWs), surface bands in semiconductors, etc. Here, we can observe nonvanishing tunneling current arising due to the presence of localized states, while the initial bands do not overlap.

The above peculiarities of tunneling phenomena in STM contacts clearly demonstrate that we have to employ an adequate method to analyze the STM/STS measurement results based on a contemporary description of tunneling processes in nanosystems. Usually, when describing tunneling processes in STM/STS, we use the standard formula for tunneling current [8]

$$I \sim 2\pi e \int \mathrm{d}\omega \, T^2 \nu_k(\omega) \nu_p(\omega) \left[n_p(\omega) - n_k(\omega - eV) \right], \qquad (1)$$

where T is the tunneling amplitude, $\nu_{k(p)}$ is the density of electronic states in the leads of the tunneling contact, and $n_{k(p)}(\omega)$ are the electron Fermi distribution functions in the contact leads. At the same time, numerous STM/STS experiments have shown that the tunneling processes on nanometer scales and, as a consequence, the resulting STM images cannot always be analyzed within the framework of the standard theory of tunneling phenomena that uses equilibrium distribution functions of tunneling particles. The application of a consistent theory allowed us to describe the tunneling processes in nanosystems with relaxation in all details.

The relaxation processes in small-sized systems diminish the tunneling current. This phenomenon was observed in numerous experiments at decreased temperatures and invariable characteristics of the tunneling contact [9]. The most general expression for the tunneling current must account for various relaxation mechanisms and a possible change in the occupation numbers, as well as the influence of the localized states. We discuss these issues below within the theoretical models that describe tunneling processes in ultrasmall contact areas.

In the present review, we analyze several key results obtained in STM/STS experiments, which were not fully explained in the framework of the standard tunneling theory guided by the equilibrium distribution of tunneling particles. Effects observed in several tunneling experiments are analyzed using contemporary ideas on tunneling phenomena that take into account the reconstructed spectrum of electronic states, the influence of nonequilibrium processes, and the presence of localized states. We discuss fundamentals of the self-consistent tunneling theory that can be applied in experiment. The theory not only allows describing numerous effects in STM/STS experiments but also predicts new results.

2. Experimental results

2.1 Charge-density waves and induced conductivity

One of the experimental results obtained by the STM/STS method that was not possible to be clearly explained within the standard theory of tunneling processes is the observation of an ordered arrangement on the molecular film surface of a liquid crystal (LC) polymer [10]. Here, the authors considered a bilayer of the LC AP-10 comb-like polymer 66 Å thick deposited on an atomically smooth conducting substrate. Using atomic force microscopy (AFM), they obtained on the surface of a defect-free region of the molecular film a relief image with a two-dimensional lattice with sides of length $a \simeq b \simeq 11.9$ Å and long diagonal of length $d \simeq 20$ Å. At the same time, using the STM method allowed them to find in the current images of the surface a periodic superstructure at the voltage difference of 5 mV, corresponding to a lattice with parameters $a^* \simeq b^* \simeq 25.5$ Å and $d^* \simeq 20.2$ Å, exceeding those of the lattice obtained in the AFM image. Changing the sign of the potential applied to the tunneling junction, we found out that the current STM image of the surface experienced the opposite phase change (Fig. 1a). Protrusions and deeps on the STM image changed, which could be explained by a CDW type distributed surface charge. Moreover, in the considered system 'conducting substrate–LC–STM tip' (Fig. 2), two types of current–voltage characteristics (CVCs) were obtained. At large distances between the tip and the surface, the CVC showed a wide band gap of ~ 5 eV (Fig. 1b), while the Fermi level E_F was inside the energy gap.

When changing the applied voltage in the range of 1.5 V to 5 mV, as well as when reducing the distance between the tip and the LC surface, the band gap almost disappeared, while conductivity sharply increased (by at least two orders of magnitude). A detailed analysis of the electronic and atomic (molecular) structures of the LC surface showed the existence of charge-density waves on the surface. In this case, the Fermi level resided inside an energy gap whose width depended on electron–phonon and electron–electron interactions, while a minimal period of the charge superstructure coincided with a length of the larger diagonal of the lattice corresponding to the relief AFM image. At the same time, it was necessary to find conditions under which observing CDWs was possible at room temperature ($kT = 25$ meV) and the tunneling voltage $V \simeq 5$ mV, as well as to explain a sharp change in system's conductivity. In order to observe CDWs, we need to have an energy gap of more than kT; otherwise, the thermal fluctuations break the CDW. Consequently, observing CDWs was impossible without local interactions between electronic states of the conducting STM tip and the LC surface.

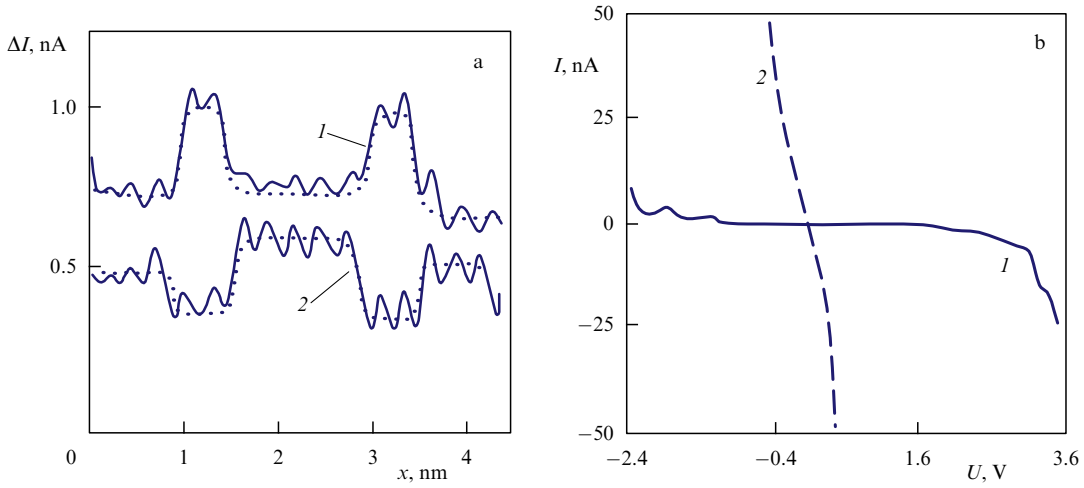

Figure 1. (a) Sections of the charge superstructure image opposite in sign to the tunneling voltage (curve *1* corresponds to $V = +5$ mV, and curve *2* corresponds to $V = -5$ mV). (b) Current–voltage characteristics at large (*1*) and small (*2*) distances between the STM tip and the surface; x is the distance along the surface.

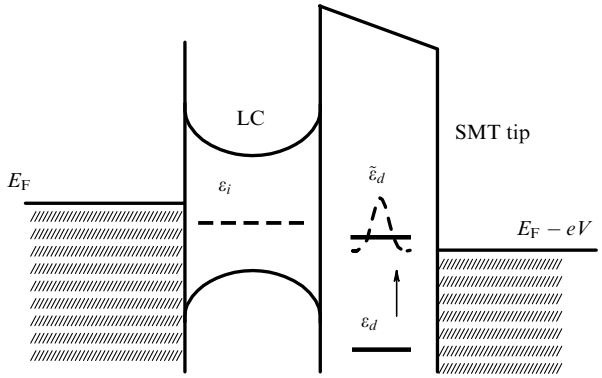

Figure 2. Schematic of the tunneling junction substrate–LC–barrier–tip. E_F is the Fermi level, ε_i are the resonance levels, ε_d is the energy of the tip localized state, and $\tilde{\varepsilon}_d$ is the bound state energy.

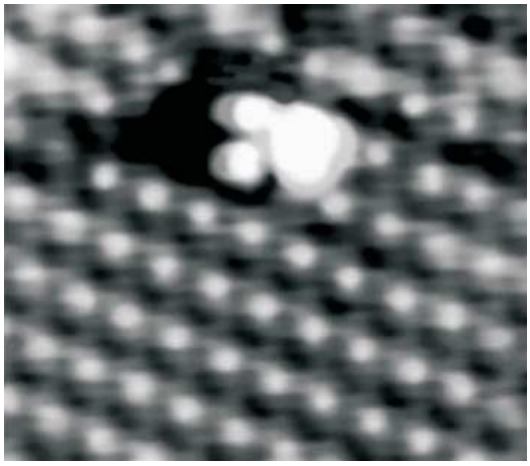

Figure 3. STM image of the As sublattice and the atomic cluster on InAs(110) surface. Scanned region is 4.4×4.4 nm. Tunneling current is 20 pA, and tip voltage $V = -0.5$ V.

In order to explain the observed effects, it was required to construct a theoretical model taking into account the presence of localized sites in the tunneling contact area. Indeed, localized states with energy ε_d much less than E_F are possible on the STM tip or LC surface. Their existence can be explained either by a break of the periodic structure at the end of the STM tip or by the presence of defects and inhomogeneities on the surface. As a result of strong hybridization between electronic states of the tip and the sample, a bound state arises with the energy $\tilde{\varepsilon}_d$ in the energy gap that changes the type of the tunneling conductance.

A self-consistent tunneling theory in nanostructures with bound localized states is considered in Section 5.

2.2 Peculiarities of the electronic structure of pure semiconductor surfaces

The STM/STS method is basically used to study the atomic and electronic structures of pure surfaces in an ultrahigh vacuum, when uncontrolled adsorbed layers do not disturb the initial surface structure. At room temperature, when carrier relaxation can be disregarded, while tunneling goes from occupied states of the STM metal tip, a reconstruction of the electronic spectrum, as a rule, has little effect on STM images of the periodic surface structures. The role of the relaxation processes increases with decreasing temperature and the tunneling transition rate may exceed the relaxation rate. As a result, a nonequilibrium distribution of tunneling particles emerges in the contact area, which essentially changes the initial density of states and yields nonequilibrium charges.

A similar effect has been observed in many experiments [9, 11]. In particular, it was considered in all details in Ref. [9], where the authors used the STM/STS method to study the InAs(110) atomically smooth surface and the region over the atomic cluster formed on the surface (Fig. 3). The measurements were done at liquid-helium temperature. The sample was the single-crystalline InAs of n-type conductivity doped with Sn atoms (5×10^{17} cm^{-3}).

In those experiments carried out over the atomically smooth surface an increase in width of the band gap Δ to 1.8 eV, compared to that for a bulky crystal (0.43 eV), was observed (Fig. 4). At the same time, the Fermi level shifted from the conduction band edge to the band gap, despite the high degree of doping. The measurements over the atomic cluster revealed a sharp decrease in the band gap width compared to values found over a smooth surface. In the case

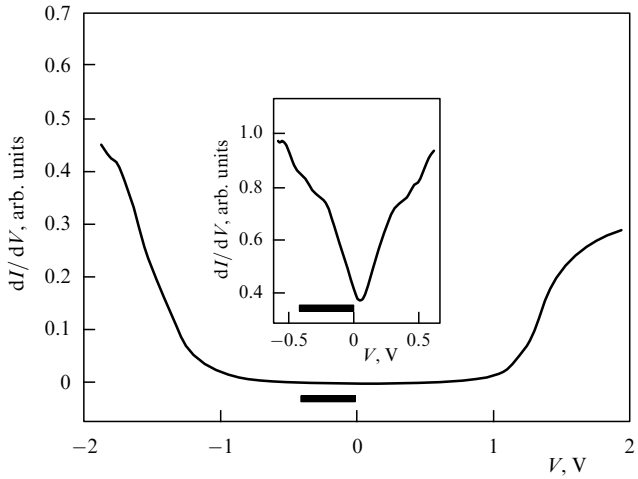

Figure 4. Tunneling conductance measured over the atomically clean surface of InAs(110) and over a three-atom cluster (shown in the inset plot). Bold horizontal line shows the position of the band gap width for the bulky crystal, equal to 0.43 eV.

of a three-atom cluster, it is given by 0.40 eV. In another experiment with a six-atom cluster, this value was equal to 0.55 eV. However, the Fermi level in these cases is inside the band gap (see Fig. 4).

Observed experimental results can be related to the fact that the nonequilibrium charge localized on the tip causes an additional bending of bands on the semiconductor surface. Over the cluster, a charge localized on the tip may be decreased or even compensated for by a nonequilibrium charge of opposite sign. Thus, a width measured over the cluster is diminished.

2.3 Microscopy and spectroscopy of isolated impurity states on semiconductor surfaces

Peculiarities of the STM method applied to the study of atomic impurities and defects were already demonstrated in the first studies of charged states of Si donor atoms on the GaAs surface [12]. In this paper, the STM image of positively charged Si donor impurity was observed at a depth up to two nanometers under the surface. Atomic images obtained at room temperature manifested themselves on the surface as protrusions of radius ~ 2.5 nm. Their height depended on the voltage applied to the STM tunneling junction. Their analysis assumed an additional bending of bands caused by the Coulomb potential of the STM tip.

Possible applications of the STM method to study impurity states at low temperatures were demonstrated for Te atoms [13]. The results obtained in this paper showed that nonequilibrium effects related to localized states must be properly accounted for. A GaAs single crystal doped by Te atoms (with a concentration of 5×10^{17} cm^{-3}) was studied. Tellurium is a donor substitutional impurity in the arsenic sublattice which loses five electrons returning to the valence band once they are bound in the GaAs crystal lattice. Its ionization energy is ~ 6 meV, which corresponds to forming a shallow donor level in the band gap of GaAs, and a theoretical estimate for the localization radius of the outer s-electron yields ~ 7 nm. It follows that the image of the Te atom substituting the As atom at the lattice site must be spherically symmetric with a radius encircling ~ 15 periods of the GaAs lattice. STM images of atoms in the upper subsurface layers were observed as spots with a localization radius of approximately 4 nm (Fig. 5). Because an STM image is defined by the outer 5s-orbitals of Te with an additional electron, as opposed to the semiconductor matrix, while nonlocalized conduction electrons contribute to the image, the image size should decrease with increasing location depth of atoms under the surface.

When a positive potential is applied to the STM tip, the images are surrounded by Friedel oscillations resulting from screening by electrons of the charge localized on the Te impurity atom (Fig. 5a).

Figure 6 shows an STM image of a Te atom in the first subsurface layer surrounded by oscillations with a period of 3.3 nm, which does not meet the estimate obtained from the standard screening model for a rigid material. According to this model, the oscillation period should be equal to half the Fermi wavelength $\lambda_F/2 \simeq 10.5$ nm. However, the influence of nonequilibrium effects and localized states in the tunneling contact area modifies the electron density distribution near an impurity atom, causes local bending of bands, and changes the Friedel oscillation period.

STM is the only method that allows us to find the form, symmetry, and space localization of impurities in the semiconductor matrix. As a typical example, Fig. 7 displays STM images of impurity atoms Te, Zn, and Mn on an

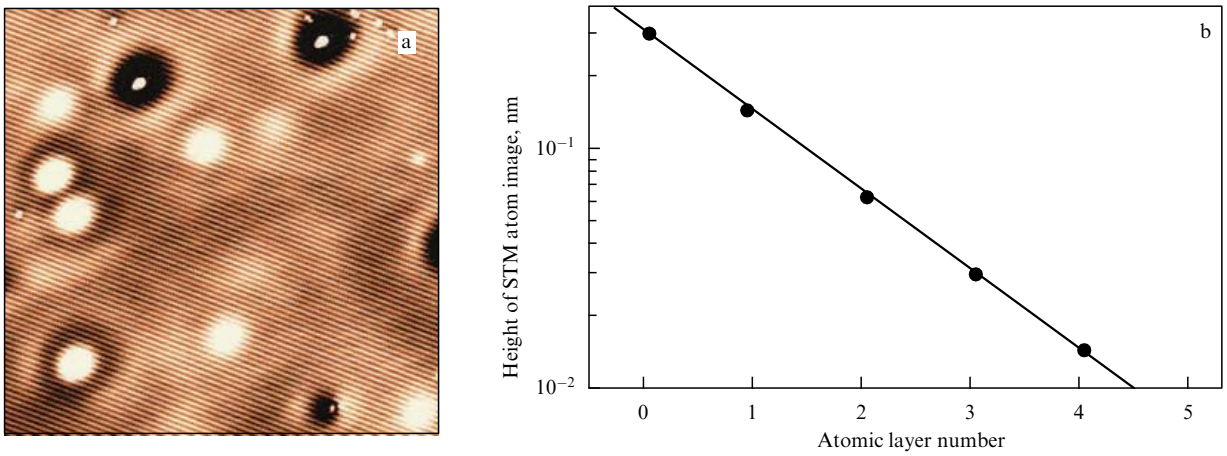

Figure 5. (a) STM images of Te atoms on the GaAs(110) surface, tip potential +1.5 V, tunneling current 60 pA. The scanned area size is 40 × 40 nm. (b) Dependence of the image amplitude of Te atoms on the location depth.

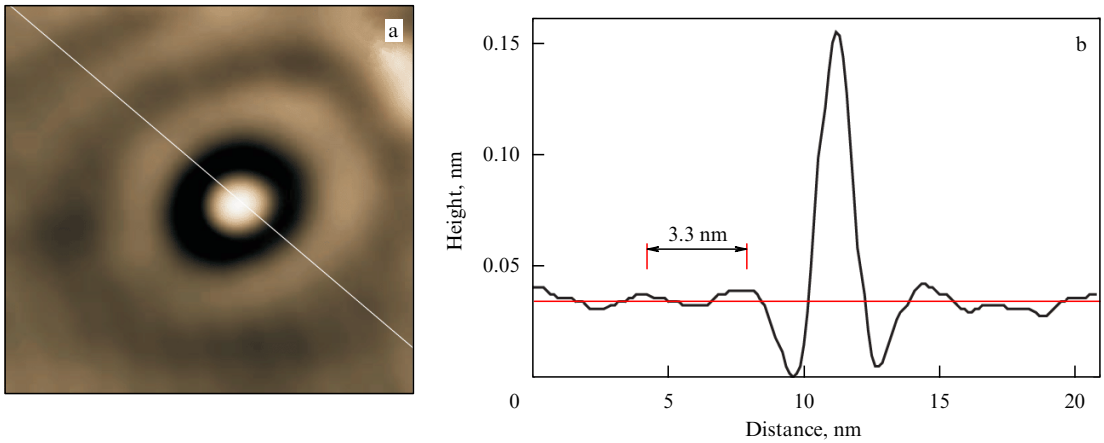

Figure 6. (a) STM image of a Te atom obtained at the tip voltage +1.5 V. (b) STM image relief along the line shown in figure (a).

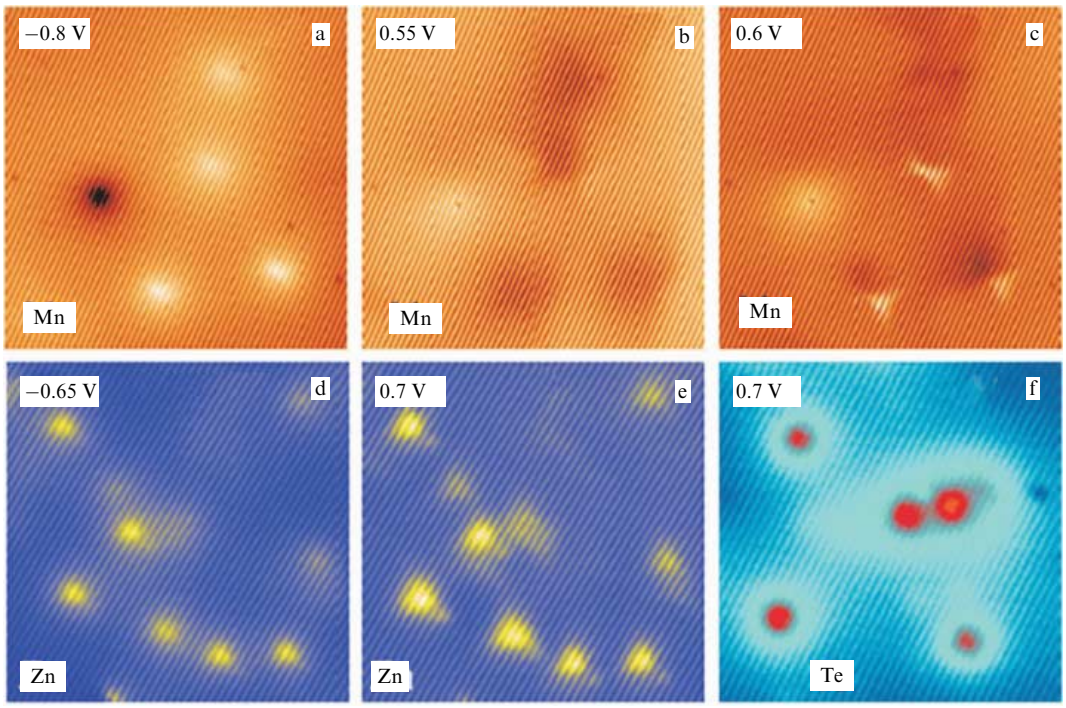

Figure 7. STM images of impurity atoms on the surface and in the subsurface layers of InAs(110): (a–c) Mn, (d, e) Zn, and (f) Te. Tunneling voltage values are shown in the figures. Frame sizes: (a–c) 40 × 40 nm, (d, e) 30 × 30 nm, and (f) 27 × 27 nm.

InAs(110) surface and on the subsurface layers for different voltage values. The images are different in shape, symmetry, and localization radius of the impurity state. In particular, most Zn atom images are in the shape of an equilateral triangle (Fig. 7e) for the unoccupied state, and of a circularly symmetric shape for occupied states (Fig. 7d). The STM images of Te atoms are circularly symmetric (Fig. 7f), regardless of the voltage and the location depth. The STM images of Mn atoms vary in a complicated way, depending on the tunneling voltage and subsurface layer where the atom is located.

The STM image amplitude (at constant applied voltage) for most studied impurities exponentially decreases with increasing impurity location depth (see Fig. 5). At a high impurity concentration, when the average distance between them does not substantially exceed the impurity state localization radius, such a dependence is influenced by a volume charge distribution. In the experiment, images can be obtained under the surface at depths up to ten atomic layers. This allows using STM as subsurface tunneling nanotomography. For spherically symmetric images of impurity atoms (for example, Te atoms), we can find how the impurity state localization radius R depends on the subsurface layer depth N, where an impurity atom is located. However, an interaction of localized states of the tip and impurity atom should also be taken into account, as should the influence of relaxation processes and nonequilibrium effects.

STM image analysis shows that different types of atomic defects cannot always be correctly identified by using a direct comparison of their images, which depend on the tunneling junction parameters. In these cases, the key properties of defects, their differences, or their identity, as well as the

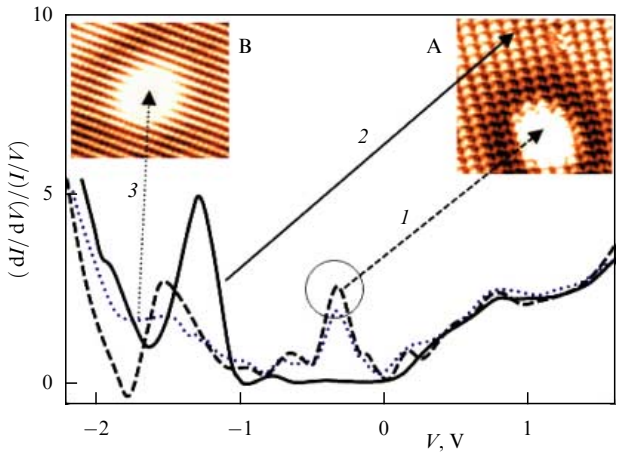

Figure 8. STM Te atom images on the first (A) and second (B) subsurface layers of GaAs(110) and the dependence of normalized tunneling conductivity on the voltage at the sample: *1* and *3* over atoms A and B, respectively, and *2* over the defect-free region of the surface. Circle shows peaks that retain their positions in the tunneling conductivity spectra at various location depths of Te atoms.

peculiarities of interactions, can be defined by analyzing the tunneling conductance spectra. Figure 8 demonstrates spectra of normalized tunneling conductivity measured for Te impurity states in the first and second subsurface layers. Here, the band gap width depends on the relative position of the impurity atom and the STM tip. The band gap boundaries near the impurity atom are shifted by 0.1–0.2 eV with respect to the value corresponding to the clean surface case. We note that if the transverse size of the tunneling contact is comparable to or less than the impurity state localization radius, the tunneling current and conductivity in such a system can basically be defined by this localized state and how it interacts with the STM tip.

The impurity Te atoms in Fig. 8 are characterized by peaks in the spectra of normalized tunneling conductivity at the voltage of ~ -0.7 V, which are absent in the measurements over the clean surface. These peaks basically retain their positions in the tunneling conductivity spectra at different location depths of Te atoms. Over the clean surface (at more than 5 nm from the impurity atom), there is a peak of the tunneling conductivity in the voltage range from -1.5 V to -1 V related to the localized state of the tip. Its position and amplitude depend on the distance between the impurity atom and the STM tip.

There are general patterns in the tunneling conductivity spectra of impurity states on the semiconductor surface. As shown above in the plots of tunneling spectra for all studied impurities and for a clean semiconductor surface, the band gap is shifted and its width is different from that of the volume band. This effect is related to the charge-induced bending of bands arising on the localized impurity state and/or on the STM tip as a result of a finite relaxation time of tunneling electrons.

There are peaks in the band gap and on its edges in the tunneling conductivity plots measured above impurity atoms (independently of their charge sign). It is the Coulomb interaction of localized charges that is responsible for the tunneling conductivity behavior. It affects the impurity initial state levels with respect to the boundaries of the band gap. The local density of states in the vicinity of the impurity atom substantially varies deep inside the band gap as well. Particularly, the density of states decreases at energies on the order of 2 eV for Te and Si donor impurities, while it increases within the valence band for the Zn acceptor impurity.

The tunneling conductivity measured directly in the localized impurity atom region has shown that for each impurity state (at least in the semiconductor matrix) the local tunneling conductivity spectrum has some specific features attributed to a given kind of atom. This makes it possible to develop a technique for STM/STS measuring of the impurity constituents based on identification of characteristic details in the tunneling conductivity spectra. It allows identifying impurity atoms using their spectral features [14].

The effect of a localized STM-probe state on the images of impurity states and atomic defects is clearly manifested when observing the abrupt change in image contrast of impurity atoms in the process of scanning along the surface [9]. For this purpose, an experiment which investigates the effect of STM-tip charge state changes on the images of localized impurity states on a semiconductor surface was conducted. Figure 9 shows STM images of the same impurity atom Te, obtained for different voltages applied to the sample. For a negative

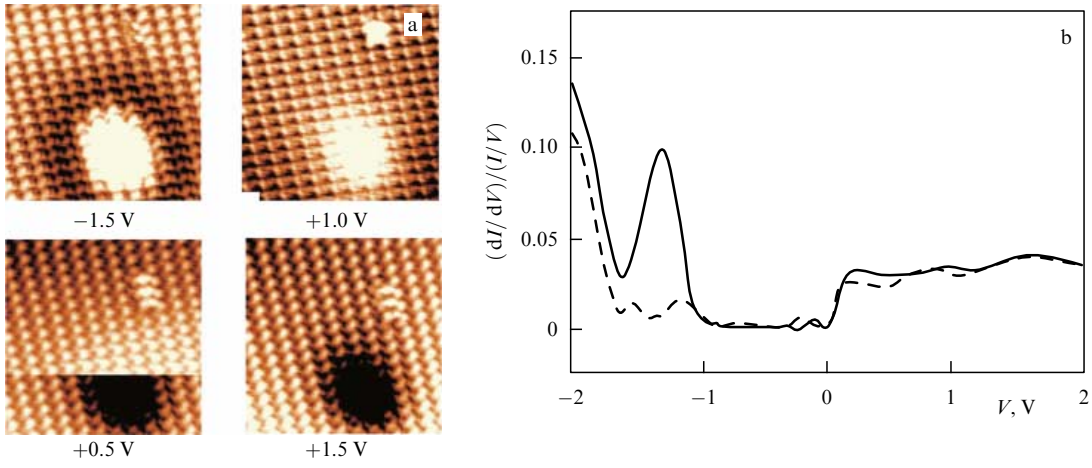

Figure 9. STM image of an impurity Te atom (a) at different voltages on the sample. The abrupt change in the image contrast at $+0.5$ V corresponds to the abrupt change in the energy of the localized state (b) at the tip of the STM probe. In figure (b), the solid dashed line indicates the measured spectra of normalized tunnel conductivity above the defect-free surface region before and after the switching in contrast of the image.

potential on the sample, the electrons in the near-surface region screen the charge of the impurity atom, inducing Friedel oscillations around the atom. Such oscillations are absent in the case of a positive potential on the sample.

At some point in the process of scanning along the surface, the contrast of the impurity atom image changes abruptly. The bright spot in the region of atom localization changes to dark. However, images of the surface atomic rows to the right and left of the impurity atom image do not undergo any switching or discontinuity. A further increase in the positive voltage does not change the contrast of the image. After an abrupt change, the contrast of the STM image returns to its original value, if the sign of the applied voltage is changed. These facts indicate that differences in the contrast of STM images do not result from a 'double' point of the STM or any other mechanical instability, but are caused by an abrupt change in the localized charge on the tip.

The key influence of localized states of the probe tip on STM images is illustrated by the two curves of normalized tunneling conductivity in Fig. 9b. Both measurements were performed before and after the abrupt change in contrast on atomically smooth and defect-free sections of the surface. The peak in tunneling conductivity near the edge of the band gap at -1.2 V disappears after the switching in the STM image. This means a change in energy of the localized state of the STM tip, which in turn leads to a modification of the nonequilibrium charge localized at the tip, resulting from the change in contribution of nonequilibrium electrons to the tunneling current. The change in the charge at the tip leads to a local band bending on the surface in the contact region and causes a change in the STM image of the impurity state.

STM/STS precision methods make it possible to analyze formation details of the spatial and energy structures of isolated dangling bonds on the surface and to study the charge states of impurity atomic orbitals in the depth of semiconductors [15]. In Ref. [16], the STM images of spatial localization of a dangling bond of the impurity atom Cr were obtained. The dangling bond arises upon replacing the As-node in the lattice of InAs on the surface and in the subsurface structure of the charge state of the orbitals of impurity atoms of Sn and Mn. In the InAs upper atomic layer, a region of increased electron density of 0.5–0.6 nm near the Cr atom was observed. Its shape corresponds to the spatial localization of an unpaired electron located in the hybrid orbital of the Cr atom dangling bond with the corresponding (upper) In atom. The perturbing potential induced by the transition metal impurity atom is limited by the size of the crystal lattice period. The detected prolate shape of the electron cloud and its dependence on the tunnel voltage reveal the spatial orientation typical of the hybrid orbital of the d-electron state.

An estimate of the localized electron Coulomb repulsion energy for this state gives a value comparable to the width of the band gap, which leads to an energy level shift observed in the tunneling conductivity spectra of the deep impurity states.

2.4 Nonequilibrium interaction of impurity states

Impurity states can greatly alter the local electronic structure on the surface and at the interfaces of semiconductors. If the distance between impurities is comparable to their localization radius, strong correlation effects change the electronic properties of such a system and have a significant effect on its tunneling conductivity. These effects, driven by nonequilibrium interaction of impurity states, drastically affect the tunneling conductivity as well as the tunneling current in the localization region of each interacting atom, whenever the applied potential is varied. The tunneling over an atom (impurity state) in such a system can repeatedly get 'switched on' or 'switched off', depending on the applied potential, increasing or decreasing part of the tunneling current flowing through each impurity state.

The first observation of local effects in the nonequilibrium interaction of two impurity states was carried out by the STM/STS method in Ref. [17]. In the experiment, the spatial distribution of normalized tunneling conductivity over the GaAs(110) surface near the interacting silicon impurity atoms was studied for various potentials at the tip of the STM probe. To obtain the spatial distribution of the tunneling conductivity along the entire surface of the investigated nanostructure, a technique for discrete measurement of the derivative of tunneling current with respect to the voltage was used. This technique made it possible to measure the tunneling conductivity spectrum over an area of less than 0.1 nm^2. In experiments, a splitting of opposite spin electron states up to the energy on the order of 1 eV was obtained in a controlled manner. Such a splitting cannot be achieved in superstrong fields by traditional methods. The investigated sample was a GaAs single crystal doped with mutually compensating impurities of Si and Zn with concentrations of 5×10^{18} and 2×10^{19} cm^{-3}, respectively. After cleaving the crystal, a region of two identical impurity Si atoms separated by a distance of 3 nm was selected on the cleavage surface, which corresponds to a doubled localization radius of the Si impurity state. The measurements were carried out at a temperature of 4.2 K.

The interaction of impurity states was studied by measuring the tunneling conductivity $(\mathrm{d}I/\mathrm{d}V)/(I/V)$ on a surface area of 10×10 nm near the interacting Si atoms. Similar measurements were carried out on an isolated Si atom for comparison. Figure 10 shows the dependence of the normalized tunneling conductivity on the applied voltage in the range from $+2.5$ to -1 V, measured along direction X indicated by arrows in the topographic STM image for one isolated atom and for two interacting impurity atoms a and b. It should be noted that the contribution from other doping impurities near the investigated impurity Si atoms was observed only in the form of a distributed inhomogeneous Coulomb potential in the crystal. This potential caused the

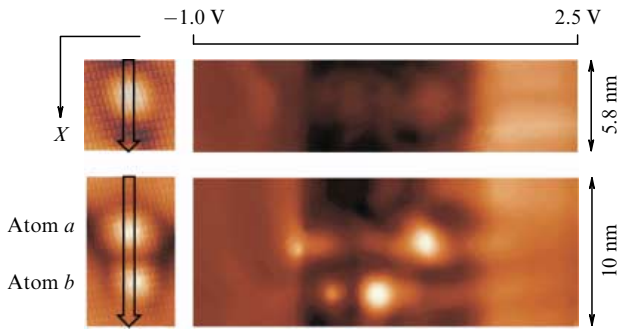

Figure 10. Upper part of the figure displays STM images of an isolated atom (on the left) and a map of the normalized local tunneling conductivity distribution near the impurity atom, measured along the X-direction shown by the arrow. The lower part of the figure displays STM images of interacting atoms a and b (on the left) and a map of the normalized local tunneling conductivity distribution near impurity atoms, measured along the X-direction.

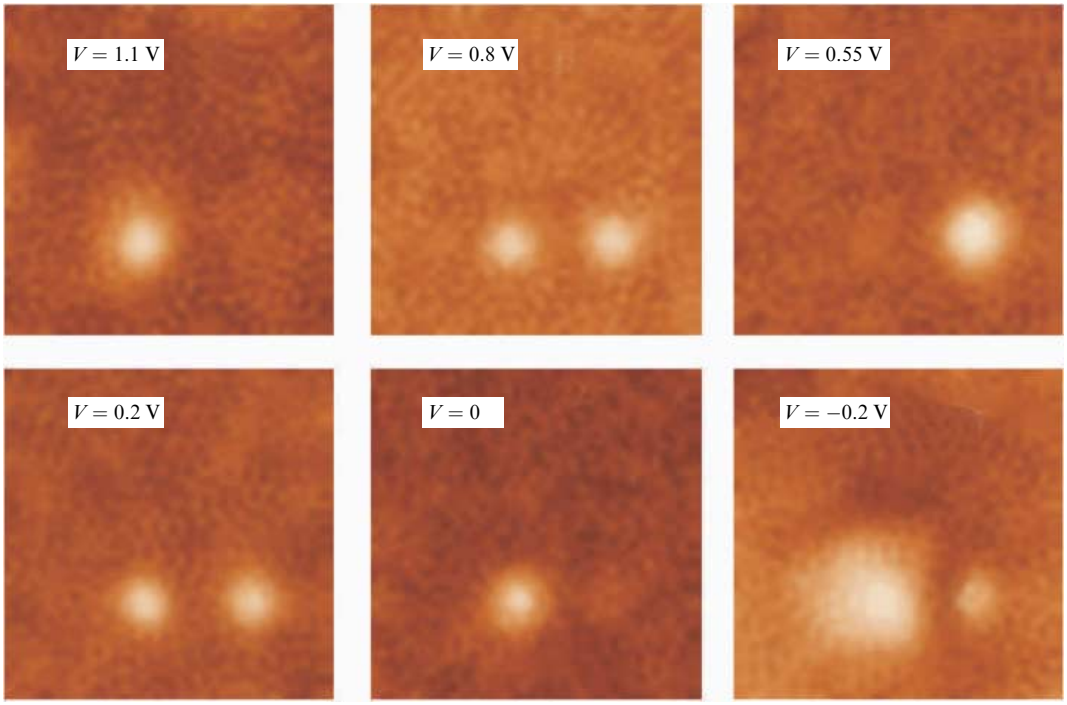

Figure 11. Images of the normalized tunneling conductivity in a 10 × 10-nm GaAs (110) surface area near interacting silicon impurity atoms separated from each other by a distance of 3 nm for the key potentials at the tip of an STM. Images are taken from Fig. 10 for selected tunneling voltages. The above tunneling conductivity distributions are not normalized, so that the contrast of images only illustrates a relative values for the minimum and maximum densities of states.

asymmetry of the initial state of the interacting pair of Si atoms, which was observed in the difference between the STM/STS images of these atoms at zero voltage across the transition area.

In the experimentally observed spatial distribution of local tunneling conductivity, two 'switching on' and 'switching off' episodes of each state associated with atoms a and b are seen when the tunneling voltage changes. In the vicinity of each of these atoms, after 'switching on', there is an excess of tunneling conductivity within the voltage range of 0.6–0.7 V, which is much greater than the width of the energy level of the localized state. The transition from one state to another for atoms a and b takes place when the voltage varies within the interval on the order of 0.15 V, which is comparable to the width of the energy level of the localized state. At the same time, in the vicinity of an isolated impurity Si atom, there are no characteristic features that clearly appear in the region of two interacting atoms.

Figure 11 displays the spatial distributions of the normalized tunneling conductivity near the interacting atoms a and b for the potentials at the STM tip corresponding to the key states of these atoms. The sequence of these images shows the energy dependence of the regions of mutually overlapping electron densities (obtained frame by frame), from which the 'on' and 'off' moments of switching the interaction, as well as the electronic state symmetry, are determined. The magnitude of the state overlap depends on the applied potential and, consequently, can be controlled by an external electric field.

The tunneling conductivity map (see Fig. 11) allows us to analyze the behavior of the local tunneling density of states near each atom and makes it possible to determine its relationship with the states of interacting electrons with a given energy.

The explanation for these effects can be given in the framework of models similar to the one used by Anderson [18], which takes into account the Coulomb interaction between electrons, as well as the effect of the tunneling potential on the position of the energy levels of impurity atoms (see Section 6, Fig. 14). The interaction of the impurity states with those of the continuous spectrum is assumed to be not too small, such that the change in the impurity state energy via the Coulomb interaction of the localized charges is governed by the mean values of occupation numbers for a fixed value of the applied potential.

This situation differs from the effects driven by the Coulomb blockade associated with the discreteness of the localized state occupation numbers. Indeed, the Coulomb blockade, in the presence of both an intraatomic Coulomb interaction and an interatomic interaction, causes the appearance of peaks in the tunneling conductivity spectrum with a change in the voltage across the contact, whose width is on the order of the width of the level of localized states (and does not exceed 0.1 eV). However, the presence of a tunneling interaction between impurity atoms can lead to a redistribution of the localized charge between atoms and to the effect of tightening the energy levels of the localized states with respect to each other in a certain interval of applied voltage. As a result, to adequately describe the experimental data obtained, it is necessary to take into account the following factors.

The appearance of an excess of the local tunneling conductivity in the vicinity of an impurity atom is observed if $|\varepsilon_{a(b)}(V) - E_{\mathrm{F}}| < \Gamma$ (Γ is the broadening of the localized atom level, and $\varepsilon_{a(b)}$ is the impurity atom energy levels). In this case, if the applied voltage exceeds the width of the level, $|eV| > \Gamma$, then the local tunneling conductivity can increase in passing the energy of the localized state through both the

Fermi level E_{SF} of the sample and the Fermi level of the tip, $E_{TF} = E_{SF} - eV$.

The Coulomb interaction of localized electrons can be described using the self-consistent mean-field approximation in the Anderson model. This approximation is quite applicable when the energy $U_{a(b)}$ of the localized electrons' Coulomb interaction at impurity levels does not greatly exceed critical value U_{cr}. Therefore, the Coulomb interaction of localized electrons within a certain range of applied voltage can lead to the appearance of two different energy states for electrons with opposite spins on a separate impurity atom.

The presence of interaction between atoms leads to a more complicated distribution of localized charges over the STM contact region. There is a significant redistribution of the localized charge between atoms, so that it is possible to stabilize the energy levels of one of the atoms near the Fermi level of the sample or the tip and tighten the energy levels with respect to each other.

Taking into account these factors makes it possible to explain the observed effects and allows constructing theoretical models to predict nontrivial phenomena arising in interactions of localized states formed by atoms, atomic defects, quantum dots, etc. This will be discussed in Section 6. A practical possibility of controling the electronic structure of a system of interacting atoms was demonstrated for the first time in these experiments. For each interacting atom, the resonant tunnel current channel can be repeatedly switched 'on' or 'off', depending on the applied potential in such a system. These effects can become a basis for the implementation of new elements of semiconductor nanoelectronics based on the use of isolated and interacting impurity atoms in a semiconductor matrix.

2.5 Nonequilibrium effects and multiparticle d-orbital interaction of impurity atoms

The appearance of nonequilibrium charges in the tunnel junction region containing impurity atoms can greatly change the initial local density of states and the tunneling conductivity spectra in the presence of Coulomb interactions. Such changes may also result from changes in the tunnel amplitudes upon rapid Coulomb potential activation, which arises in the presence of nonequilibrium occupation numbers on the impurity atom. This situation is analogous to the effect of the appearance of power-law singularities in the metal X-ray absorption spectra [19]. Singularities manifest themselves in STM experiments if the rate of tunnel transitions from energy level of the deep impurity atom to the STM probe metal tip significantly exceeds the relaxation rate of nonequilibrium distribution of the electron occupation numbers on the impurity atom, and its energy level is empty. As a result, the Coulomb interaction between the charged impurity and the conduction electrons sharply engages, leading to a change in the tunnel amplitude value.

The response of the conduction electrons in the metal tip of the STM probe to the abrupt change in Coulomb potential is essentially different from the one-particle picture. In this case, one can expect the formation of power-law singularities in the current–voltage characteristics, when the magnitude of the applied potential approaches the value of the impurity atom energy level. An attempt to describe the appearance of a singularity in the current–voltage characteristics was first made in Ref. [20]. The authors, however, confined themselves to qualitative arguments on the renormalization of the tunnel amplitude, using the well-known result [19], which led to wrong conclusions and which will be discussed in more detail in Section 7.

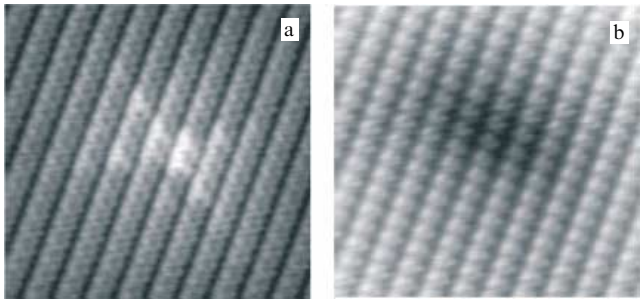

Figure 12. STM image of the Mn impurity state on the InAs(110) 5 × 5 nm surface at voltages across the sample $V_s = -0.5$ V (a) and $V_s = +0.7$ (b).

Similar effects were observed in the STM study of Cr and Mn impurity states on the InAs(110) surface [21]. Singular features were most clearly manifested in low-temperature STM/STS studies of impurity Mn atoms. Figure 12 shows the STM images of the surface relief near the doping Mn atom for different values of the tunnel voltage. A bright image (protrusion) of a cross-like shape was observed for the negative voltage V_s on the sample within the localization region of the Mn impurity state, which turned into a dark oval image (dip) at a positive voltage V_s.

The dependence of the normalized tunneling conductivity on the potential and the current STM images in the localization region of the Mn impurity state is shown in Fig. 13. At a negative voltage across the sample, a cross-like image persists in the range $-1 < V_s < -0.5$ V, which corresponds to the electron density of the d-orbitals hybridized to the states of the InAs lattice for the Mn impurity atom in the valence band (Fig. 13a–c). At low voltages this impurity state exhibits a filling close to a single one. When the applied voltage approaches the value corresponding to the energy ε_d of the acceptor level, in the voltage range $|eV - \varepsilon_d| < \Gamma$ the tunneling conductivity increases in the region of localization of the d-orbitals. Parameter Γ corresponds to the broadening of the energy level ε_d caused by interaction with the states of the continuous spectrum of the semiconductor valence band and the states of the STM probe. As a result, in the localization region of the Mn impurity atom, the tunneling current and the local tunneling conductivity increase due to an increase in the local density of states in the semiconductor. This density of states directly reflects the nonspherical symmetry of the localized impurity d-level. An additional amplification of the tunneling current and conductivity arises upon involvement of nonequilibrium Coulomb interaction between the impurity and the charge carriers in the region of the tunnel junction.

The Coulomb interaction of a positively charged impurity atom and conduction electrons at voltages close to the energy of the localized state leads to the following dependence of the tunneling current on the voltage:

$$I(V) \sim \frac{\gamma_k \gamma_p}{\gamma} \left[\frac{D^2}{(eV - \varepsilon_d)^2 + \gamma^2} \right]^{|W|\nu}, \qquad (2)$$

where W is the average value of the impurity atom Coulomb potential, $\gamma = \gamma_k + \gamma_p$ ($\gamma_{k(p)}$ is the rate of tunneling transitions to the leads of the tunnel junction), ν is the density of electronic states at the tip of the STM probe, and D is the

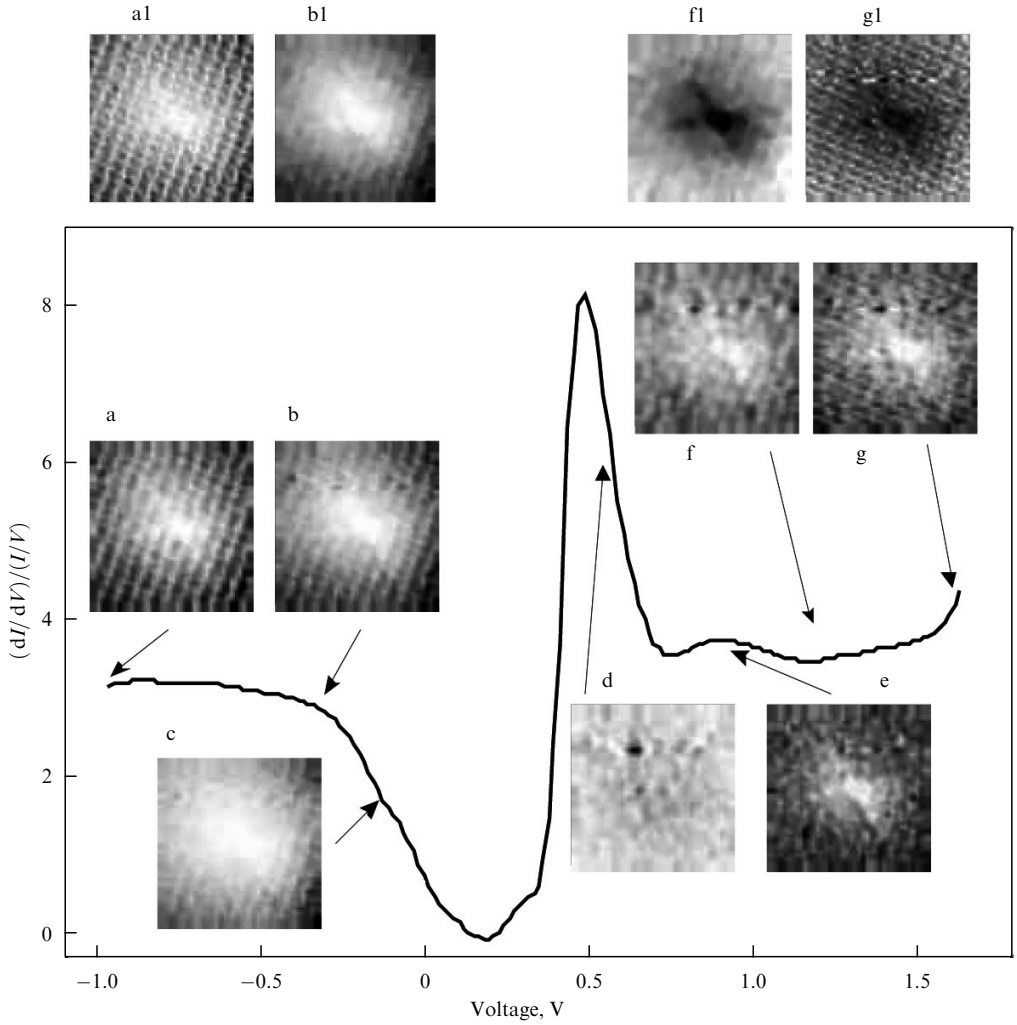

Figure 13. Normalized tunneling conductivity and current STM images in localization region of the Mn d-orbital impurity state. Insets a–g correspond to the spatial distribution of normalized tunneling conductivity for different values of the bias voltage. The bias voltages corresponding to the insets are indicated by arrows. Insets a1–g1 show images of current spatial distribution ($I(V)$) for voltages corresponding to insets (a, b, f, g) located directly under the current STM images.

conduction band width in the metal. One can expect, therefore, an additional increase in the tunnel current value in the vicinity of the impurity atom, whenever the voltage at the contact approaches threshold value $eV = \varepsilon_d$.

Figure 13 shows the increase in tunneling conductivity in the vicinity of an impurity atom as the voltage applied across the tunnel junction approaches the value of the energy of the localized state. Clearly, the peak in the tunneling conductivity in the neighborhood of the impurity level is not governed by the Kondo effect, since the voltage across the tunnel junction (~ 400 meV) exceeds the energy level width of the impurity atom (~ 100 meV). If the potential difference across the tunnel contact is near zero, the cross-like structure of the local density of the impurity state becomes unresolved in STM images of the surface section shown in Fig. 13. For the voltage in the ranges $-1 < V < -0.3$ V and $0.5 < V < 1.5$ V, a bright spot is clearly present in the spatial distribution of the local tunneling conductivity in the vicinity of the impurity atom. On the other hand, it should be stressed that within the voltage range $0.5 < V < 1.5$ V the impurity atom takes the form of a dark spot for the tunneling current spatial distribution, which corresponds to a local decrease in its magnitude.

Thus, the Coulomb interaction between the impurity state and the conduction electrons for continuous spectrum states at the STM tip significantly changes the tunneling amplitudes and leads to the formation of characteristic features in the tunneling current and in the tunneling conductivity, when the magnitude of the applied voltage approximates the energy of the impurity atom. In this case, the current–voltage characteristics may have an asymmetric form due to the different dependences of the phase factor on the applied voltage: below or above the threshold voltage. Therefore, by changing the distance between the tip of the STM probe and the surface, it is possible to vary the behavior of the current–voltage characteristics.

3. Tunneling processes peculiarities in low-dimensional structures

The results of modern experimental studies of tunneling processes in low-dimensional structures or in mesoscopic systems, and especially in nanoscale structures, cannot be treated within the framework of the standard theory of tunneling phenomena based on the use of the equilibrium distribution function of tunneling particles. It is implicitly

assumed that the nonequilibrium particle relaxation rate is much higher than the tunneling rate. To adequately describe the tunneling processes in such STM structures and contacts, consideration of relaxation processes along with the reconstruction of the electronic spectrum within the contact leads and the influence of localized states should be properly taken into account.

A general approach to the description of these processes can be based on the use of the Keldysh diagram technique, which makes it possible to take into consideration in a self-consistent manner both the renormalization of the initial spectrum of the system due to tunneling processes and the relaxation of nonequilibrium particles [22].

This approach includes the model Hamiltonian of the following system:

$$\hat{H} = \hat{H}_0 + \hat{H}_{\text{imp}} + \hat{H}_{\text{tun}} + \hat{H}_{\text{int}} , \tag{3}$$

where the Hamiltonian $\hat{H}_0$ describes the isolated leads of the tunnel junction:

$$\hat{H}_0 = \sum_{\mathbf{k}\in \text{L},\,\sigma} \varepsilon_k c^+_{\mathbf{k}\sigma} c_{\mathbf{k}\sigma} + \sum_{\mathbf{p}\in \text{R},\,\sigma} (\varepsilon_p - eV) c^+_{\mathbf{p}\sigma} c_{\mathbf{p}\sigma} , \tag{4}$$

$c^+_{\mathbf{k}(\mathbf{p})\sigma}/c_{\mathbf{k}(\mathbf{p})\sigma}$ are the creation/annihilation operators for non-interacting electrons with momenta $\mathbf{k}(\mathbf{p})$ and energies $\varepsilon_{k(p)}$ on the left L (sample) and right R (STM-probe tip) leads of the tunnel contact, respectively.

The Hamiltonian $\hat{H}_{\text{imp}}$ corresponds to impurity states localized in the region of the tunnel junction and accounts for the Coulomb interaction of localized electrons:

$$\hat{H}_{\text{imp}} = \sum_{d,\,\sigma} \varepsilon_d d^+_\sigma d_\sigma + U \sum_{d,\,\sigma} n^\sigma_d n^{-\sigma}_d . \tag{5}$$

In this expression, $n^\sigma_d = d^+_\sigma d_\sigma$, the operator $d^+_\sigma (d_\sigma)$ corresponds to the creation/annihilation of an electron with spin σ at the impurity level, and U is the magnitude of the Coulomb interaction of electrons at the energy level of the localized state. Tunneling processes through an intermediate state between the contact leads are generally described by the Hamiltonian

$$\hat{H}_{\text{tun}} = \sum_{\mathbf{k},\,d,\,\sigma} T_{\mathbf{k}d} (d^+_\sigma c_{\mathbf{k}\sigma} + c^+_{\mathbf{k}\sigma} d_\sigma) + \sum_{\mathbf{p},\,d,\,\sigma} T_{\mathbf{p}d} (d^+_\sigma c_{\mathbf{p}\sigma} + c^+_{\mathbf{p}\sigma} d_\sigma) . \tag{6}$$

It is usually assumed that the tunneling amplitudes $T_{k(p)d}$ do not depend on the momentum and describe the transitions of electrons from one lead of the tunnel junction to the other through intermediate localized states. The Hamiltonian $\hat{H}_{\text{int}}$ describes the presence of various kinds of interactions in the system, such as that with a thermostat, the electron–phonon interaction, the interaction of localized electrons with conduction electrons in the tunnel junction leads, and so on.

Let us start with a model system described by Hamiltonian (3), in which the term $\hat{H}_{\text{int}}$ is absent, and the leads of the tunnel junction are in thermodynamic equilibrium. The expression for the tunneling current can be written out using the Keldysh diagram technique for nonequilibrium processes:

$$I(V) = \text{i} \sum_{\mathbf{k},\,\sigma,\,d} T_{\mathbf{k}d} (c^+_{\mathbf{k}\sigma} d_\sigma - d^+_\sigma c_{\mathbf{k}\sigma}) = 2\,\text{Re} \sum_{\mathbf{k},\,\sigma,\,d} T_{\mathbf{k}d} G^{\sigma<}_{\mathbf{k}d}$$
$$= -2\,\text{Re} \sum_{\mathbf{p},\,\sigma,\,d} T_{\mathbf{p}d} G^{\sigma<}_{\mathbf{p}d} . \tag{7}$$

The last equality is a consequence of the continuity equation. The Green's functions in the Keldysh diagram technique are determined in a standard way by using Dyson equation [23]. In fact, in order to find the tunneling current, it is sufficient to find only functions $G^<_{dd}$ and G^{A}_{dd}, which are related as follows:

$$G^<_{dd}(\omega) = (-\text{i}) 2 n_d(\omega)\,\text{Im}\, G^{\text{A}}_{dd}(\omega) . \tag{8}$$

In this case, the tunneling current is given by

$$I(V) = 2\text{i}\gamma_k \int (\text{i} G^<_{dd} - 2 n_k\,\text{Im}\, G^{\text{A}}_{dd}) \frac{\text{d}\omega}{2\pi} , \tag{9}$$

where $\gamma_{k(p)d} = \nu^0_{\text{L(R)}} \pi T^2_{k(p)d}$, and G^{A} is the advanced Green's function. In this approach, the presence of localized electrons in the Coulomb interacting system leads to a self-consistent change in the retarded Green's function G^{R}_{dd}.

In many cases, to correctly describe tunneling phenomena, it is necessary to take into account both the renormalization of the electronic spectrum and the finite relaxation rate of nonequilibrium electrons in the contact leads in a self-consistent manner. To model the relaxation, we can introduce an additional interaction with the thermostat into the Hamiltonian:

$$\hat{H}_{\text{int}} = \sum_{\mathbf{k}\mathbf{p}'\sigma} g(\mathbf{k} - \mathbf{p}') c^+_{\mathbf{k}\sigma} b_{\mathbf{p}'\sigma} + \text{h.c.} , \tag{10}$$

where

$$g(\mathbf{k} - \mathbf{p}') = \frac{1}{L^d} \int g(r) \exp\left[\text{i}(\mathbf{k} - \mathbf{p}')\mathbf{r}\right] \text{d}\mathbf{r} , \tag{11}$$

$g(r)$ is the effective matrix element of the interaction with the thermostat, $g(r) \to 0$ in the region of the tunnel barrier and on its boundaries, $b^+_{\mathbf{p}'\sigma}$ is the creation operator of an electron in the thermostat in the state $(\mathbf{p}'\sigma)$, L is the characteristic size of the system, and d is its dimension. The thermostat resides in a state of equilibrium that does not change under perturbation $g(r)$.

Now, the equations for the Green's function in the Keldysh technique contain an additional intrinsic energy part of $\hat{\Sigma}$, caused by the interaction with the thermostat:

$$\Sigma^{\alpha\beta}_{\mathbf{k}\mathbf{k}'} = \sum_{\mathbf{p}'} g(\mathbf{k} - \mathbf{p}')\, g^+(\mathbf{k}' - \mathbf{p}')\, G^{\alpha\beta}_{\mathbf{p}'\mathbf{p}'}(\omega) . \tag{12}$$

It is reasonable to assume that the thermostat is a system of randomly located scatterers at points $\mathbf{R}_i$ [or $g(r)$ is a random function] and

$$g(\mathbf{k} - \mathbf{p})\, g(\mathbf{k}' - \mathbf{p}) = N^{-1} \sum_i g_i^2 \exp\left[\text{i}(\mathbf{k} - \mathbf{k}')\mathbf{R}_i\right] . \tag{13}$$

For the continuous spectrum states under a chaotic distribution of such centers, one obtains

$$\Sigma^{\alpha\beta}_{\mathbf{k}\mathbf{k}'} = g_i^2 \bar{n} \delta_{\mathbf{k}\mathbf{k}'} \sum_{\mathbf{p}'} G^{\alpha\beta}_{\mathbf{p}'}(\omega) , \tag{14}$$

where $\bar{n} = N_i/N$ is the average concentration of scatterers, and

$$\frac{\partial n_k}{\partial t} + \text{i} T_k \int \text{d}\omega \left(G^<_{dk}(\omega) - G^<_{kd}(\omega)\right) = -2\Gamma_k (n_k - n^0_{p'}) , \tag{15}$$

$$\Gamma_k = g_i^2 \pi \bar{n} \nu_{p'}(\omega) . \tag{16}$$

However, if one is interested in the current contribution from the bound states localized near the microcontacts of states, then we can choose another limiting case for the thermostat model, namely, its local activation. In this case, $\hat{\Sigma}_{kk'}$ does not depend on k and k', i.e.

$$\Sigma^{\alpha\beta}_{\mathbf{kk}'} = g^2 \sum_{\mathbf{p}} G^{\alpha\beta}_{\mathbf{pp}}(\omega)\,, \quad \Sigma^{\mathrm{R}}_{\mathbf{kk}'} = \mathrm{i}\pi g^2 \nu_{\mathbf{p}}(\omega) = \mathrm{i}\Gamma_{\mathbf{k}}(\omega)\,. \tag{17}$$

We will give more detail on the last case.

An explicit form of the retarded Green's function $\hat{G}^{\mathrm{R}}$ can be found within the framework of this model. For example, the following relations hold true:

$$G^{\mathrm{R}}_{dd}(\omega) = \frac{1 - \mathrm{i}\Gamma_k N(\omega)}{Z(\omega)}\,, \tag{18}$$

$$Z(\omega) = \big(1 - \mathrm{i}\Gamma_k N(\omega)\big)\big(\omega - \varepsilon_d + \mathrm{i}\gamma_p(\omega)\big) - T_k^2 N(\omega)\,, \tag{19}$$

where

$$N(\omega) = \sum_{\mathbf{k}} G^{\mathrm{R}0}_{\mathbf{kk}}(\omega)\,, \tag{20}$$

$$\Sigma^{r}_{dd} = \mathrm{i}\pi |T_p|^2 \nu_{p'}(\omega) = \mathrm{i}\gamma_p(\omega)\,, \tag{21}$$

where $\nu_{p'}(\omega)$ is the density of electronic states p'.

From the explicit form of the Green's function, it is possible to determine the conditions for the formation of bound states being split off from the boundary of the original spectrum due to the tunneling interaction [24].

4. Bound states split off from boundaries of the original spectrum by tunneling interaction

The spectrum of the investigated system is determined by the poles of the Green's function G^{R}_{dd}. If the broadenings of the electronic states γ_p and Γ_k are small, the collective bound state energy in the band gap is given by

$$\omega - \varepsilon_d - T_k^2 N(\omega) = 0 \tag{22}$$

or

$$\omega - \varepsilon_d - T_k^2 \int \mathrm{d}\varepsilon\, \frac{\nu_0(\varepsilon)}{\omega - \varepsilon} = 0\,, \tag{23}$$

where $\nu_0(\varepsilon)$ is the bare density of states in the continuous spectrum. Equation (23) has a purely real solution in the regions $\omega > \varepsilon_v$ and $\omega < \varepsilon_0$, where ε_0 and ε_v are the lower and upper bounds of the spectrum ε_k, respectively. The value of ω corresponds to a localized state lying in the band gap. The energy of this state depends on the value of T_k and on the specific form of bare density of states $\nu_0(\varepsilon)$.

If the approximate expression $\nu_0(\varepsilon) = (\varepsilon_v - \varepsilon_0)^{-1}$ is taken for the density of states of a two-dimensional electron system, then, in the region $\omega > \varepsilon_v$, one has

$$\omega = \tilde{\varepsilon}_d = \omega_0 + \varepsilon_v\,, \tag{24}$$

$$\omega_0 = (\varepsilon_v - \varepsilon_0) \exp\left[-\frac{(\varepsilon_v - \varepsilon_0)(\tilde{\varepsilon}_d - \varepsilon_d)}{T_k^2}\right]. \tag{25}$$

For a quasi-one-dimensional character of $\nu_0(\varepsilon)$ near the boundary of the spectrum, we have

$$\tilde{\varepsilon}_d = \varepsilon_v + \left(\frac{T_k^2}{\varepsilon_v - \varepsilon_d}\right)^2 W_1^{-1}\,, \tag{26}$$

where W_1 is the effective width of the quasi-one-dimensional band. It is easy to see that the amplitude of the wave function ψ_0 of the bound state in the contact region is determined by the residue of function $G^{\mathrm{R}}(\omega, 0) = \sum_{kk'} G^{\mathrm{R}}_{kk'}(\omega)$ at the pole $\omega = \tilde{\varepsilon}_d$.

This gives

$$a^D |\psi_0|^2 = \left[\int \mathrm{d}\varepsilon\, \nu_0(\varepsilon)(\tilde{\varepsilon}_d - \varepsilon)^{-1}\right]^2 \left[\int \mathrm{d}\varepsilon\, \nu_0(\varepsilon)(\tilde{\varepsilon}_d - \varepsilon)^{-2}\right]^{-1}, \tag{27}$$

where a is the lattice constant, and D is the spatial dimension of the system. In the case of a two-dimensional band one finds

$$|\psi_0|^2 = (\varepsilon_v - \varepsilon_d)^2 W_2 \omega_0 T_k^{-4} a^{-D}\,, \tag{28}$$

where $W_2 = \varepsilon_v - \varepsilon_0$ is the width of the $2D$ band.

It turns out that, even though an exponential reduction in the tails of the wave function takes place at the characteristic length $R_0 \approx a(W/\omega_0)^{1/D}$, the size of the effective localization region is not determined by R_0, but by the value of $(|\psi_0|^{-2})^{1/D}$.

5. Appearance of induced tunneling conductivity

The presence of split-off bound states may lead to the appearance of induced tunneling conductivity. In the stationary case, focusing on the contribution to the tunneling current from the bound state, we can assume that

$$G^{<}_{\mathbf{kk}'}(\omega) = -2\mathrm{i} n_k(\omega)\, \mathrm{Im}\, G^{\mathrm{R}}_{\mathbf{kk}'}(\omega)\,, \tag{29}$$

$$G^{<}_{dd}(\omega) = -2\mathrm{i} n_d(\omega)\, \mathrm{Im}\, G^{\mathrm{R}}_{dd}(\omega)\,, \tag{30}$$

where $n_k(\omega)$ and $n_d(\omega)$ are occupation numbers for states k and d, respectively.

The tunneling current is given by

$$\begin{aligned} I &= -2\int \frac{\mathrm{d}\omega}{2\pi}\, \gamma_p(\omega)\, \mathrm{Im}\, G^{\mathrm{R}}_{dd}(\omega)\big(n_d(\omega) - n^0_p(\omega)\big) \\ &= 2\int \frac{\mathrm{d}\omega}{2\pi}\, \Gamma_k(\omega)\, \mathrm{Im}\, G^{\mathrm{R}}(\omega, 0)\big(n_k(\omega) - n^0_{p'}(\omega)\big)\,, \end{aligned} \tag{31}$$

where

$$\mathrm{Im}\, G^{\mathrm{R}}(\omega, 0) = \mathrm{Im} \sum_{\mathbf{kk}'} G^{\mathrm{R}}_{\mathbf{kk}'}(\omega)\,, \tag{32}$$

and $n^0_{p'}(\omega)$ is the Fermi distribution function for states p' with energy ω. Distributions of $n^0_p(\omega)$ and $n^0_{p'}(\omega)$ differ in the position of the Fermi level.

For the case of a two-dimensional system of electrons, by taking into account that for $\omega \sim \tilde{\varepsilon}_d$ one arrives to

$$\sum_{\mathbf{kk}'} \mathrm{Im}\, G^{\mathrm{R}}_{\mathbf{kk}'}(\omega) = \mathrm{Im}\, G^{\mathrm{R}}_{dd}(\omega)(\varepsilon_v - \varepsilon_d)^2\, T_k^{-2}\,, \tag{33}$$

we obtain the following expression for the tunneling current in the approximation $T_k^2 \nu_0 \gg \gamma_p, \Gamma_k$:

$$I \sim \frac{2\gamma_p \Gamma_k \big(n^0_{p'}(\tilde{\varepsilon}_d) - n^0_p(\tilde{\varepsilon}_d)\big)}{\big[\Gamma_d T_k^2 (\varepsilon_v - \varepsilon_d)^{-2} + \Gamma_k\big] Z'(\tilde{\varepsilon}_d)}\,, \tag{34}$$

where $Z'(\tilde{\varepsilon}_d)^{-1} = (T_k \nu_0)^{-2} \exp\left[-(\varepsilon_v - \varepsilon_d)\varepsilon_v T_k^{-2}\right]$.

Quantities γ_p and Γ_k entering formula (34) are determined for $\omega \sim \tilde{\varepsilon}_d$. If $\tilde{\varepsilon}_d$ lies between E_{F} and $E_{\mathrm{F}} - eV$, the tunneling

current is different from zero due to the appearance of a new collective state $\tilde{\varepsilon}_d$.

We recall once again that the position of $\tilde{\varepsilon}_d$ with respect to the boundary of the band depends on the applied voltage V. This is due to the difference between characteristic energies being changed additionally by the value of eV. It should be noted that, even in the absence of localized states in the contact region, the presence of a finite relaxation rate of nonequilibrium carriers leads to a modification of expression (1) for the tunneling current. In this case, taking into account the carrier relaxation processes, the formula for the tunneling current acquires the form [25]

$$I \sim 2\pi e \int \mathrm{d}\omega \, \frac{T^2 v_k(\omega) v_p(\omega) \left[n_p(\omega) - n_k(\omega - eV)\right] \Gamma_k \Gamma_p}{T^2 v_p \Gamma_p + T^2 v_k \Gamma_k + \Gamma_p \Gamma_k} \,. \quad (35)$$

Here, $\Gamma_{k(p)}$ are the carrier relaxation rates in the contact leads, and T is the amplitude of the tunneling transitions between the contact leads. When $\Gamma_{k(p)} \gg T^2$, the expression transforms to standard formula (1). Relaxation in the system reduces the tunnel current, while a change in the local density of states and the appearance of a nonequilibrium local electron distribution in the region of the tunnel junction can significantly distort its spectral characteristics. Consequently, the current is determined by the weakest link in the chain in the presence of relaxation.

It is possible to modify the results obtained for a model of a thermostat with chaotically distributed scatterers. Note that for such a model one has

$$\Sigma^{\alpha\beta}_{\mathbf{k}\mathbf{k}'} = g_i^2 \bar{n} \delta_{\mathbf{k}\mathbf{k}'} \sum_{\mathbf{p}} G^{\alpha\beta}_{\mathbf{p}}(\omega) \,, \quad (36)$$

where $\bar{n}$ is the scatterer mean number per unit cell.

In contrast to the formulas in which the tunneling current is determined by the relaxation rate in the local electron density

$$I \sim \int \mathrm{d}\omega \, (n_k - n_p^0) \, \mathrm{Im}\, G^{\mathrm{R}}(\omega, 0) v_p(\omega) g^2 \,, \quad (37)$$

the tunneling current now determines the rate of change of the particle total number:

$$I \sim \int \mathrm{d}\omega \, v_p(\omega) g^2 \bar{n} (n_k - n_p^0) \, \mathrm{Im} \sum_{\mathbf{k}} G^{\mathrm{R}}_{\mathbf{k}\mathbf{k}}(\omega) \,. \quad (38)$$

It turns out that near the energy of the split-off level, expressions (37) and (38) differ by $\bar{n}|\psi_0|^{-2}$, where ψ_0 is the amplitude of the wave function of the bound state at point $r = 0$. Consequently, if the concentration $\bar{n}$ of relaxation centers is such that, in the region of localization of the bound state $S \sim |\psi_0|^{-2}$ there is only one such center on average, then both expressions determining the tunneling current simply coincide.

Thus, when analyzing modern STM/STS experiments, it is necessary to substantially modify the familiar description of tunnel contacts [26]. The idea that tunneling current value reflects the initial density of states in the material becomes incorrect. A change in the local density of states and the appearance of electron nonequilibrium distribution are possible even in the absence of localized states. In this case, terms $\hat{H}_{\mathrm{imp}}$ and $\hat{H}_{\mathrm{int}}$ are absent in Hamiltonian (3), while the tunneling processes between the contact leads are described by Hamiltonian $\hat{H}_{\mathrm{tun}}$:

$$\hat{H}_{\mathrm{tun}} = \sum_{\mathbf{k},\,\mathbf{p},\,\sigma} T(c^+_{\mathbf{k}\sigma} c_{\mathbf{p}\sigma} + c^+_{\mathbf{p}\sigma} c_{\mathbf{k}\sigma}) \,. \quad (39)$$

A change in the local density in the contact leads $\nu_{\mathrm{L(R)}}$ can be determined using the Keldysh diagram technique as follows [27]:

$$\nu_{\mathrm{L(R)}} = \frac{1}{\pi} \, \mathrm{Im} \sum_{\mathbf{k},\,\mathbf{k}' \in \mathrm{L(R)}} G^{\mathrm{A}}_{\mathbf{k},\mathbf{k}'} = \frac{\nu^0_{\mathrm{L(R)}}}{1 + T^2 \nu^0_{\mathrm{L}} \nu^0_{\mathrm{R}}} \,. \quad (40)$$

A locally nonequilibrium distribution of electrons can be found from the expression

$$\sum_{\mathbf{k},\,\mathbf{k}' \in \mathrm{L}} G^{<}_{\mathbf{k},\mathbf{k}'} = \frac{2\mathrm{i}\nu^0_{\mathrm{L}}}{(1 + T^2 \nu^0_{\mathrm{L}} \nu^0_{\mathrm{R}})^2} \left(n_k(\omega) + T^2 \nu^0_{\mathrm{L}} \nu^0_{\mathrm{R}} n_p(\omega)\right)$$
$$= 2\pi \mathrm{i} n_{\mathrm{L}} \nu_{\mathrm{L}} \,, \quad (41)$$

where ν^0_{L} and ν^0_{R} are unperturbed densities of states in the left and right leads of the tunnel junction, $n_{k(p)}(\omega)$ are equilibrium Fermi distribution functions for electrons in the leads of the tunnel junction, and ν_{L} and ν_{R} are local densities of states in the contact region, when tunneling transitions are taken into account.

As a result, the expression for the tunneling current reads

$$I = \int \mathrm{d}\omega \, \frac{4T^2 \nu^0_{\mathrm{L}} \nu^0_{\mathrm{R}}}{(1 + T^2 \nu^0_{\mathrm{L}} \nu^0_{\mathrm{R}})^2} \left[n_k(\omega) - n_p(\omega)\right] \,. \quad (42)$$

Thus, the interaction of a sample with a closely spaced tip during tunneling makes the initial density of states distorted, and in some cases new bound states appear that play a particularly important role in dielectrics, CDWs on the surface, surface bands in semiconductors, etc. At a potential difference, when the original bands do not overlap, a nonzero current can be observed. A contribution to the current from impurities with energy levels lying deep below the Fermi level appears. In particular, in low-dimensional systems, an induced tunneling current can appear at voltages corresponding to the energy of the band gap, due to the localized states split off from the boundaries of the spectrum [see Eqn (34)].

The fact that the position of a bound state depends on the value of tunneling matrix element T in a complicated way implies a nonexponential (and sometimes nonmonotonic) dependence of the tunneling current on the distance to a sample in a potential region on the order of the energy of such states. This model of tunneling processes involving split-off localized states makes it possible to explain many experimental data, for example, a sharp increase in the tunneling conductivity when observing CDWs on the surface of an LC and a distance decrease between a sample surface and an STM tip, described in Section 2.1.

6. Anderson model for describing nonequilibrium impurity states with correlated electrons

In this section, we analyze the experimental spectra of tunneling conductivity based on the nonequilibrium interaction of impurity states. The behavior of tunneling conductivity over a wide range of voltages from +2.5 V to −2 V (the typical value of the Kondo temperature does not exceed 1 meV) was investigated in the STS experiments described in

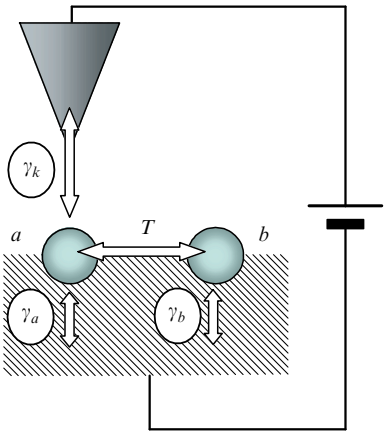

Figure 14. Schematic presentation of the tunnel structure in the presence of interacting impurities.

Section 2.4. Therefore, the influence of the Kondo effect on the formation of tunneling characteristics is negligible. The investigated system is put into a weak magnetic field **B**, so that the splitting of levels does not exceed their broadening.

Coulomb interaction of electrons localized on impurity atoms is taken into account in a self-consistent manner using the mean-field approximation. It turns out that if the limiting voltage across the contact changes, the difference in energy for electrons of opposite spins on each impurity atom can greatly increase. A sharp increase in spin asymmetry occurs as well, leading to a transition from the 'paramagnetic' regime to the 'magnetic' one. A further increase in the applied voltage makes a reverse transition from the 'magnetic' state to the 'paramagnetic' one also possible. In addition, the conditions under which the interaction between impurity atoms leads to an enhancement of the magnetic regime in a nonequilibrium state are revealed. The interaction between impurity atoms also gives rise to a redistribution of nonequilibrium charges localized near impurities. Therefore, the stabilization of impurity levels becomes possible in the vicinity of the Fermi level for any contact leads, as well as the mutual approaching of interacting impurity energy levels in a certain range of applied external voltages.

If two simple atoms a and b are located near the surface of a semiconductor and the STM tip is located above atom a (Fig. 14), the tunneling transitions between the localized states of atom a and the STM tip are determined by the tunneling rate γ_k. The transition rates between localized states on impurity atoms a and b and states of a continuous spectrum of a semiconductor are characterized by the corresponding kinetic parameters γ_a and γ_b.

Kinetic parameters γ_a, γ_b, and γ_k are determined from the Hamiltonian of the investigated structure. The interaction between impurity atoms leads to a direct 'hopping' of an electron from one atom to another with the corresponding transition amplitude T. Energies of impurity atoms a and b at zero voltage across the contact are different, since atom a manifests itself in the STS spectra at $V = 0$, while atom b does not (see Section 2.4, Fig. 11). The difference between the positions of levels of localized states can be caused both by the inhomogeneous potential of the crystal lattice of a semiconductor and by the arrangement of atoms in different near-surface layers of the semiconductor matrix. Differences between the energies of localized states of impurity atoms can lead to different energy values of the intrasite Coulomb interaction.

The amplitude T of the electronic transition between impurity atoms does not exceed the relaxation rates γ_a and γ_b arising from hybridization of localized states with the states of a continuous spectrum of the semiconductor matrix. The reason is, according to experimental results, that the distance between the impurities studied is approximately 3 nm. This assumption means that, because of energy level broadening, their equilibrium splitting due to the interaction does not reveal itself in the density of states of the system studied. But the kinetic processes based on this interaction, leading to a redistribution of the charge between impurity atoms, are greatly modified. The presence of a weak magnetic field does not allow the resolution of energy level splitting for electrons with opposite spins in the experiment. This is because the splitting does not exceed the width of the levels ($2\mu B < \Gamma$) at low voltages across a tunnel junction (μ is the magnetic permeability).

Let us consider the peculiarities of tunnel characteristics over impurity atoms in the regime of variable valence, for which the parameters of the system satisfy the conditions $\varepsilon/\Gamma \sim 1$, $U \gg \varepsilon, \Gamma$, $2\mu B < \Gamma$. In this regime, the Coulomb interaction of localized electrons can be self-consistently accounted for in the mean-field approximation:

$$\tilde{\varepsilon}_a^{\sigma} = \varepsilon_a^{\sigma} + \alpha V + U_a \langle n_a^{-\sigma} \rangle\,, \quad \tilde{\varepsilon}_b^{\sigma} = \varepsilon_b^{\sigma} + \beta V + U_b \langle n_b^{-\sigma} \rangle\,, \quad (43)$$

$$\varepsilon_{a(b)}^{\pm\sigma} = \varepsilon_{a(b)} \mp \mu B\,. \quad (44)$$

The initial level position depends on the applied voltage as a consequence of the existence of an external electric field in the contact region (term αV, where $\alpha < 1$, takes into account approximately the influence of the external field), and due to the Coulomb interaction of localized electrons, the magnitude of which is determined by the nonequilibrium distribution of the electron density at a fixed voltage across the contact.

The impurity state occupation numbers are nonequilibrium quantities and can be self-consistently determined from the system of kinetic equations. Interactions between impurity atoms leads to the dependence of nonequilibrium occupation numbers of one of the impurity atoms ($n_a^{\pm\sigma}$) on the corresponding occupation numbers of another atom ($n_b^{\pm\sigma}$).

The Hamiltonian of the system has the form (3), in which the part $\hat{H}_{\rm imp}$ corresponds to impurity states and takes into account the Coulomb interaction of localized electrons:

$$\hat{H}_{\rm imp} = \sum_{\sigma} \varepsilon_a^{\sigma} a_{\sigma}^{+} a_{\sigma} + \frac{U_a}{2} \sum_{\sigma} n_{\sigma}^{a} n_{-\sigma}^{a} + \sum_{\sigma} \varepsilon_b^{\sigma} b_{\sigma}^{+} b_{\sigma} + \frac{U_b}{2} \sum_{\sigma} n_{\sigma}^{b} n_{-\sigma}^{b}\,. \quad (45)$$

In this expression, $n_{\sigma}^{a} = a_{\sigma}^{+} a_{\sigma}$, where operator a_{σ} annihilates an electron with spin σ at the impurity atom a, $n_{\sigma}^{b} = b_{\sigma}^{+} b_{\sigma}$, b_{σ} destroys an electron on atom b with spin σ, and ε_a, ε_b are the energy levels of impurity atoms a and b, which in general depend on the applied voltage.

$\hat{H}_{\rm tun}$ is responsible for tunneling transitions between impurity states and each of the contact leads; it has the form

$$\hat{H}_{\rm tun} = \sum_{\mathbf{p},\sigma} T_{\mathbf{p},a} (c_{\mathbf{p},\sigma}^{+} a_{\sigma} + \text{h.c.}) + \sum_{\mathbf{p},\sigma} T_{\mathbf{p},b} (c_{\mathbf{p},\sigma}^{+} b_{\sigma} + \text{h.c.}) + \sum_{\mathbf{k},\sigma} T_{\mathbf{k},a} (c_{\mathbf{k},\sigma}^{+} a_{\sigma} + \text{h.c.})\,. \quad (46)$$

Interactions between impurities are included in the term

$$\hat{H}_{\rm int} = \sum_{\sigma} T(a_{\sigma}^{+} b_{\sigma} + b_{\sigma}^{+} a_{\sigma}) \,. \tag{47}$$

Green's functions $G_{a\mathbf{k}}^{\sigma <}$, which determine the magnitude of the tunneling current, can be found from the system of kinetic equations [23].

As noted above, when using the Keldysh diagram technique, the energy part $\hat{\Sigma}$ itself may include different types of interactions. In the case of interest, however, it is reasonable to assume that $\hat{\Sigma}$ is determined by tunneling transitions between impurity states and contact leads, along with the interaction between impurities themselves only. The employment of this approximation is completely justified, since the strongest interaction in this case is the Coulomb repulsion U, which is included in the unperturbed impurity Green's function G_0.

The kinetic coefficients that determine the tunneling processes can be represented in the form

$$\begin{aligned} &\gamma_k(\omega) = \pi |T_{ka}|^2 \nu_{\mathbf{k}}(\omega) \,, \qquad \gamma_b(\omega) = \pi |T_{pb}|^2 \nu_{\mathbf{p}}(\omega) \,, \\ &\gamma_a(\omega) = \pi |T_{pa}|^2 \nu_{\mathbf{p}}(\omega) \,, \qquad \Gamma = \gamma_a + \gamma_b + \gamma_k \,. \end{aligned} \tag{48}$$

The key issue of our approach is the self-consistent condition, which must be satisfied by the nonequilibrium electron occupation numbers on the impurity atoms n_a^{σ} and n_b^{σ}:

$$n_a^{\sigma} = \frac{1}{\pi} \int \mathrm{d}\omega \, n_a^{\sigma}(\omega) \, \mathrm{Im} \, G_{aa}^{\rm A}(\omega) \,, \quad n_b^{\sigma} = \frac{1}{\pi} \int \mathrm{d}\omega \, n_b^{\sigma}(\omega) \, \mathrm{Im} \, G_{bb}^{\rm A}(\omega) \,. \tag{49}$$

The nonequilibrium occupation numbers $n_a^{\sigma}(\omega)$ and $n_b^{\sigma}(\omega)$ are determined from the system of kinetic equations, a detailed derivation of which can be found in paper [17]. The total electron density for each of the atoms of the impurity complex can be determined from the system of equations

$$\begin{aligned} n_a^{\sigma} &= n_p^{\sigma}(a) + \frac{\gamma_k(\gamma_b + \eta_{\sigma})\big(n_k^{\sigma}(a) - n_p^{\sigma}(a)\big) + \gamma_b \Gamma_{ab}}{(\gamma_k + \gamma_a)(\gamma_b + \eta_{\sigma}) + \gamma_b \eta_{\sigma}} \,, \\ n_b^{\sigma} &= n_p^{\sigma}(b) + \frac{\gamma_k \eta_{\sigma}\big(n_k^{\sigma}(a) - n_p^{\sigma}(a)\big) - (\gamma_a + \gamma_k)\Gamma_{ab}}{(\gamma_k + \gamma_a)(\gamma_b + \eta_{\sigma}) + \gamma_b \eta_{\sigma}} \,, \end{aligned} \tag{50}$$

where

$$\begin{aligned} &\eta^{\sigma} = T^2 \, \mathrm{Im} \, R_{ab}^{\sigma} \,, \\ &\Gamma_{ab} = T\gamma_k \int \mathrm{Im} \left(R_{ab} \sum_{\sigma} G_{ab}^{\mathrm{R}\sigma}(\omega) \right) \big(n_k(\omega) - n_p(\omega)\big) \, \mathrm{d}\omega \,, \\ &n_{p(k)}^{\sigma}(a) = \frac{1}{\pi} \int \mathrm{d}\omega \, n_{p(k)}^{0}(\omega) \, \mathrm{Im} \, G_{aa}^{\mathrm{A}-\sigma}(\omega) \,, \end{aligned} \tag{51}$$

and

$$R_{ab}^{-1} = G_{0a}^{\mathrm{R}-1} - G_{0b}^{\mathrm{A}-1} - \mathrm{i}\Gamma \,. \tag{52}$$

This is a system of nonlinear equations for $n_{a(b)}^{\sigma}$, because energies $\varepsilon_{a(b)}^{\sigma}$ and functions $G_{ab}^{\mathrm{R}\sigma}$, $G_{aa}^{\mathrm{R}\sigma}$, R_{ab} depend on the electron occupation numbers with opposite spins.

In the equilibrium case, $V = 0$ and, consequently, $n_a^{\sigma} = n_p^{\sigma}(a) = n_k^{\sigma}(a)$.

Substituting the nonequilibrium occupation numbers on the impurity found from the kinetic equations into the expression for the tunneling current, we obtain the final expression for the tunneling current:

$$\begin{aligned} I(V) = e \, &\frac{\gamma_k(\gamma_b + \eta_{\sigma})}{(\gamma_a + \gamma_k)(\gamma_b + \eta_{\sigma}) + \gamma_b \eta_{\sigma}} \\ &\times \int \left[\left(\gamma_a + \frac{\gamma_b \eta_{\sigma}}{\gamma_b + \eta_{\sigma}} \right) \mathrm{Im} \, G_{a,a}^{\mathrm{R}\sigma}(\omega, V) \right. \\ &\left. + T \, \frac{\gamma_b \gamma_k}{\gamma_b + \eta_{\sigma}} \, \mathrm{Im} \left(R_{ab}^{\sigma} G_{ab}^{\mathrm{A}\sigma}(\omega, V) \right) \right] \\ &\times \big(n_p^0(\omega) - n_k^0(\omega - eV) \big) \, \mathrm{d}\omega \,, \end{aligned} \tag{53}$$

where for each fixed value of the voltage across the contact, the self-consistently determined nonequilibrium occupation numbers n_a^{σ} and n_b^{σ} enter into functions G_{aa}^{R}, G_{ab}^{R}, and R_{ab}.

As expected, the tunneling current depends only on the difference between the electron distribution functions in the contact leads. The first term in the expression for the tunneling current describes the renormalization of the relaxation rate for the nonequilibrium electron density on impurity atom a due to its interaction with the neighboring impurity atom b:

$$\gamma_a \longrightarrow \gamma_a + \frac{\gamma_b \eta_{\sigma}}{\gamma_b + \eta_{\sigma}} \,. \tag{54}$$

If there is no interaction between impurity atoms, $T = 0$, $\eta = 0$, then expression (53) simply describes a current flowing through an impurity localized state [23].

The second term in formula (53) is responsible for redistribution of a charge between the interacting impurity atoms. As a result of this redistribution, the tunneling conductivity obtained from Eqn (53) is no longer proportional to the density of states on the impurity.

The considered system of two interacting Anderson impurities is the simplest example of a multichannel tunnel structure that exhibits interactions between different tunneling channels. This can lead to some interference effects, which greatly complicates the investigation of tunneling processes in such systems.

As a result of a self-consistent analysis of the proposed model, it is possible to reveal various behavior regimes in the tunneling conductivity in the vicinity of interacting impurity atoms over a wide range of voltage variations across the contact. In numerical calculations, the coefficients α and β, which describe a change in the energy of impurity levels in an external field, are valued as $\alpha \simeq 0.3$ and $\beta \simeq 0.1$.

If $\gamma_k \ll \gamma_a, \gamma_b$, then, in a certain range of values of the voltage across the contact, the energy difference for electrons of opposite spins significantly exceeds Γ. Therefore, one of the impurity atoms (atom a) can be in the 'magnetic' state. When the applied voltage is varied, the transitions from the 'paramagnetic' mode to the 'magnetic' one and vice versa may occur (Fig. 15a). As the tunneling voltage changes, such transitions lead to two-fold switching of atom a 'on' and 'off' in the spectrum of tunneling conductivity spatial distribution (Fig. 15b). This has been observed in experiments (see Section 2.4).

Yet, the energy levels of impurity atoms are stabilized in the vicinity of the Fermi level of one of the contact leads (the tip of the STM or the sample), while the voltage across the contact varies over a wide range comparable to the value of the Coulomb interaction U. In the tunneling conductivity spectrum obtained over one of the impurity atoms, two peaks appear, the width of each being comparable to the value of the Coulomb interaction and greatly exceeding the tunnel width

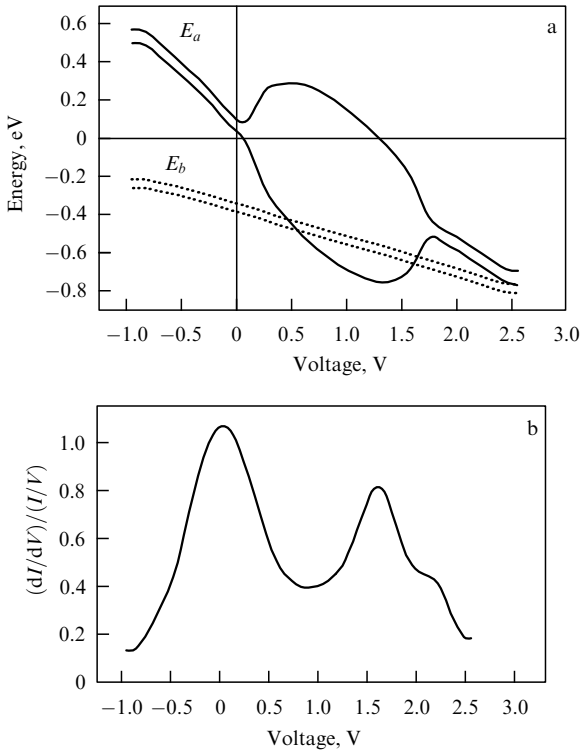

Figure 15. Two anomalously wide distinct peaks in the tunneling conductivity spectrum, which are in good agreement with experimental STS curves. (a) Dependence of the energy of atoms a and b on applied voltage. Typical values of parameters (eV) are: $\varepsilon_a^0 = -0.25$, $\varepsilon_b^0 = -0.5$, $U_a = 1.6$, $U_b = 0.5$, $\gamma_a = 0.2$, $\gamma_b = 0.2$, $\gamma_k = 0.05$, $\varepsilon_a = \varepsilon_a^0 - 0.3$, $\varepsilon_b = \varepsilon_b^0 - 0.1$; $T = 0.2$. The solid lines correspond to ε_a^σ and $\varepsilon_a^{-\sigma}$. The dashed lines correspond to the mean value of $\varepsilon_b = (1/2)(\varepsilon_b^\sigma + \varepsilon_b^{-\sigma})$, because the atom b is close to its paramagnetic state for a given set of parameters. (b) Dependence of normalized tunneling conductivity on applied voltage.

of the levels of localized states. This agrees with the experimental data given in Section 2.4.

7. Exciton-like Coulomb correlations and singularities of tunneling characteristics

At present, it is fairly well understood that for small tunneling contacts the Coulomb interaction can strongly influence the observed density of states due to the appearance of nonequilibrium charge in the contact region. Yet the effects that can be described using the mean-field approximation as in the previous section are unusual and interesting [28–31].

In addition, there is an interesting possibility of renormalization of the tunneling amplitude itself thanks to Coulomb interactions. Such a change cannot be reduced to a modification of the local density of states along with the electron distribution. In this section, it will be shown that taking into account vertex corrections in tunneling amplitudes results in the appearance of a singularity in the current–voltage characteristics [32], analogous to those that arise at the edge of X-ray absorption spectrum in metals [33]. These singularities must manifest themselves when the tunneling current flows through deep impurity states on the semiconductor surface. The most favorable conditions to develop this singularity are those under which the rate γ_k of tunneling into a metal electrode (for example, in a tunneling microscope needle) becomes larger than the relaxation rate γ_p of a nonequilibrium charge on impurity.

As will be shown for $\gamma_k \gg \gamma_p$, the impurity level becomes almost empty when the voltage across the tunneling junction exceeds the impurity energy level. In a sense, we can say that at that moment the potential of the impurity ion is 'switched on' abruptly. By analogy with the case of a step-like (in time) activation of an ion core potential upon knocking out an electron by gamma radiation, one can expect the appearance of power-law singularities in the current–voltage characteristics. To what extent this analogy really applies can be clarified by calculating within the framework of the nonequilibrium diagram technique only. Such an assumption was put forward in the work by Matveev and Larkin [20], though the authors confined themselves to qualitative reasoning on renormalization of tunneling amplitude, which led to a series of wrong conclusions.

Let us consider a semiconductor–impurity state–metal type tunneling system described by Hamiltonian (3). For simplicity, we shall consider a 'neutral single-electron' impurity. The Coulomb interaction in equilibrium makes the state of impurities single-filled. For sufficiently large tunneling constants, the Coulomb interaction on the impurity itself can be ignored if we are interested in conductivity at voltages close to the position of impurity energy level ε_d. A nonequilibrium level filling becomes small under these conditions, which suppresses intraatomic Coulomb effects. We also note that the Kondo regime is known to be irrelevant at such high voltages [34, 35] and makes no contribution to developing singularities on tunneling characteristics.

The most important thing in this problem is that the Coulomb interaction of an electron (or, more correctly, a hole) on an impurity with the conduction electrons in metal is taken into account:

$$\hat{H}_{\rm int} = \sum_{\mathbf{k}\mathbf{k}'\sigma\sigma'} W_{\mathbf{k}\mathbf{k}'} c^+_{\mathbf{k}\sigma} c_{\mathbf{k}'\sigma} (1 - c^+_{d\sigma'} c_{d\sigma'}) \,. \tag{55}$$

Hamiltonian $H_{\rm int}$ describes the scattering of conduction electrons on the ion Coulomb potential, which is no longer compensated for if the electron moves from a localized state to the contact leads. Since the Kondo regime is not formed under given conditions, it is sufficient to consider the current in the first order in tunneling amplitude T_{kd}. The Coulomb interaction with a positively charged hole on an impurity does not lead to an electron spin flip. Therefore, one can consider the tunneling amplitude renormalization for each spin independently. To simplify the expressions, we will replace the exact Coulomb interaction by a constant equal to the mean value of the screened Coulomb potential, which corresponds to taking into account the s-scattering of conduction electrons by point potential $W_{\mathbf{k}\mathbf{k}'} = W$.

The calculation of the current can be started within the framework of the nonequilibrium diagram technique with an expression written in terms of Green's function $G^<$ (in what follows, the charge of the electron is $e = 1$):

$$I(V) = \mathrm{Im}\, J(V) \,, \qquad J(V) = \mathrm{i} \sum_{\mathbf{k},\sigma} \int \mathrm{d}\omega \, T_{kd} G^{\sigma <}_{\mathbf{k}d} \,. \tag{56}$$

Here, we introduced the tunnel 'response function' $J(V)$, since this quantity gets renormalized in the Coulomb interactions.

In order not to consider separately the effect of the constant part of the Coulomb interaction and the ion core, it is simpler to move to the hole representation for electrons on impurity: $d_{\sigma'} = c^+_{d\sigma'}$. Then, the Coulomb interaction is simply

written down as

$$\hat{H}_{\rm int} = W \sum_{\mathbf{k}\mathbf{k}'\sigma\sigma'} c^{+}_{\mathbf{k}\sigma} c_{\mathbf{k}'\sigma} d^{+}_{\sigma'} d_{\sigma'} \tag{57}$$

with constant $W < 0$. We shall introduce no special notation for the hole Green's functions, by understanding G_{dd} and G_{kd} as functions with hole operators.

If one ignores the Coulomb interaction in the lowest order in T_{kd}, the usual expression for the tunneling current is immediately obtained in terms of hole Green's functions:

$$J^0(V) = \mathrm{i} \sum_{\mathbf{k},\sigma} \int \mathrm{d}\omega\, T_{kd}^2 \big(G^{\sigma<}_{\mathbf{kk}}(\omega) G^{\sigma\mathrm{R}}_{dd}(-\omega) + G^{\sigma\mathrm{R}}_{\mathbf{kk}}(\omega) G^{\sigma>}_{dd}(-\omega) \big). \tag{58}$$

Substituting the corresponding expressions for the Keldysh Green's functions and after summing over the momenta k, we obtain

$$J^0(V) = \gamma_k \int \mathrm{d}\omega \left[\frac{n_k^0(\omega)}{\omega + eV - \varepsilon_d - \mathrm{i}\gamma} - \frac{-\mathrm{i}\gamma n_d(\omega)}{(\omega + eV - \varepsilon_d)^2 + \gamma^2} \right], \tag{59}$$

where the standard rate of tunneling transitions $\gamma_k = T_{kd}^2 \nu \pi$ appeared, and ν is the density of states in the metal needle. Kinetic parameter $\gamma = \gamma_k + \gamma_p$, where γ_p corresponds to the relaxation rate of the electron distribution on the localized state. In this system, this relaxation rate is also determined by tunneling transitions, but into the bulk states of the semiconductor: $\gamma_p = T_{pd}^2 \nu_p \pi$. (Generally, other types of relaxation processes can be included in the relaxation parameter γ_p.)

Nonequilibrium occupation numbers $n_d(\omega)$ in formula (59) are electronic. These are determined from the kinetic equations for function $G^{<}$. At low temperatures, from equation (59) we obtain

$$J^0(V) = \gamma_k \left[\ln X - \mathrm{i} \left(\frac{\gamma_k}{\gamma} \operatorname{arccot} \left(\frac{\varepsilon_d - eV}{\gamma} \right) + \frac{\gamma_p}{\gamma} \operatorname{arccot} \left(\frac{\varepsilon_d}{\gamma} \right) \right) \right], \tag{60}$$

where X means

$$X = \frac{\varepsilon_d - eV + \mathrm{i}\gamma}{D}, \tag{61}$$

D is the width of the conduction band in a metal (or, more accurately, the quantity inversely proportional to the density of states ν). Setting apart the imaginary part from $\ln X$ and using formulas (56), (59), and (60) we can reproduce the usual formulas for the tunneling current:

$$J^0(V) = \gamma_k \ln |X| + \mathrm{i}\, \frac{\gamma_k \gamma_p}{\gamma} \left[\operatorname{arccot} \left(\frac{\varepsilon_d - eV}{\gamma} \right) - \operatorname{arccot} \left(\frac{\varepsilon_d}{\gamma} \right) \right]. \tag{62}$$

These expressions were written down in a somewhat nonstandard form for a connection to a subsequent rendering, since quantity $J^0(V)$ is the basis element for higher orders in perturbation theory.

Let us consider the effect of Coulomb interactions on tunneling amplitude [36]. The vertex corrections are not always small, and the results obtained near the threshold voltages (when the Fermi level in metal crosses the impurity level) using the many-particle approach differ greatly from the single-electron picture. Corrections to the tunneling amplitude are shown in Fig. 16. It is easy to see that the first correction has a logarithmic divergence near the threshold values of voltage: $eV = \varepsilon_d$. The divergence is cut off by finite relaxation rates and rates of tunneling transitions:

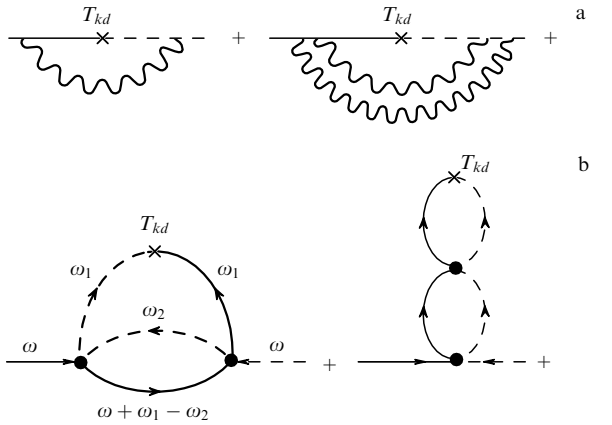

Figure 16. Coulomb corrections to tunneling amplitude T_{kd}. Solid lines designate Green's functions G_k of electrons in metal, dashed lines show the impurity Green's functions G_d. (a) Ladder approximation, and (b) parquet diagrams (Coulomb wavy lines are replaced for compactness by black dots in interaction vertices).

$$J^1(V) = \mathrm{i} \sum_{\mathbf{k},\sigma} \int \mathrm{d}\omega\, T_{kd} \big(G^{\sigma<}_{\mathbf{kk}}(\omega) G^{\sigma\mathrm{R}}_{dd}(-\omega) T^{1++}_{kd} - G^{\sigma\mathrm{R}}_{\mathbf{kk}}(\omega) G^{\sigma>}_{dd}(-\omega) T^{1--}_{kd} \big). \tag{63}$$

The effective tunnel matrix elements vary due to the Coulomb interaction as follows:

$$T^{1--}_{kd} = -\mathrm{i} T_{kd} W \sum_{\mathbf{k},\sigma} \int \mathrm{d}\omega_1 \left(G^{\sigma<}_{\mathbf{kk}}(\omega_1) G^{\sigma\mathrm{R}}_{dd}(-\omega_1) + G^{\sigma\mathrm{R}}_{\mathbf{kk}}(\omega_1) G^{\sigma>}_{dd}(-\omega_1) \right). \tag{64}$$

As we have seen in deriving formulas (58) and (59), the first combination of Green's functions in integral $G^{\sigma<}_{kk} G^{\sigma\mathrm{R}}_{dd}$ makes a logarithmically large contribution for $|\varepsilon_d - eV| \leqslant \gamma$. Therefore, even if the Coulomb interaction itself is not strong, $W\nu \ll 1$, then parameter $W\nu \ln(\gamma^2/D^2)$ can be on the order of unity or greater. The tunnel vertex T^{1++}_{kd} differs from T^{1--}_{kd} only in sign, so that we can write

$$T^{1++}_{kd} = -T^{1--}_{kd} = -T_{kd} L, \tag{65}$$

where L is expressed as

$$L = W\nu \big[\ln |X| + \mathrm{i}\Phi \big], \qquad \Phi = \frac{\gamma_p}{\gamma} \left[\operatorname{arccot} \left(\frac{\varepsilon_d - eV}{\gamma} \right) - \operatorname{arccot} \left(\frac{\varepsilon_d}{\gamma} \right) \right]. \tag{66}$$

The appearance of singularities in tunneling conductivity is most easily described in the ladder approximation shown in Fig. 16a.

The ladder diagrams can be summed up exactly, since for each pair of Green's functions the integration over frequencies can be carried out independently. Then, one obtains

$$J^{ladd}(V) = J^0(V) \big[1 + L + L^2 + \ldots \big] = \frac{J^0(V)}{1 - L}. \tag{67}$$

Using formulas (60) and (66), we obtain the following voltage dependence of the current:

$$I(V) = \operatorname{Im} J^{ladd}(V) = \gamma_k \operatorname{Im}\left[\frac{\ln|X| + i\Phi}{1 - Wv\left(\ln|X| + i\Phi\right)}\right]$$
$$= \frac{\gamma_k\gamma_p}{\gamma}\left[\operatorname{arccot}\left(\frac{\varepsilon_d - eV}{\gamma}\right) - \operatorname{arccot}\left(\frac{\varepsilon_d}{\gamma}\right)\right]$$
$$\times\left\{\left(1 - Wv\ln\left[\frac{(\varepsilon_d - eV)^2 + \gamma^2}{D^2}\right]\right)^2\right.$$
$$\left. + (Wv)^2\,\frac{\gamma_p^2}{\gamma^2}\left[\operatorname{arccot}\left(\frac{\varepsilon_d - eV}{\gamma}\right) - \operatorname{arccot}\left(\frac{\varepsilon_d}{\gamma}\right)\right]^2\right\}^{-1}. \quad (68)$$

A peak is superimposed on the ordinary stepwise dependence of current on voltage, related to the passage of a localized level, which gives rise to an additional increase in the current near the threshold voltage $eV = \varepsilon_d$. It is known that if logarithmic parameter $Wv\ln(\gamma^2/D^2)$ becomes too large, the ladder approximation 'overestimates the role' of perturbations, leading to singularities that are too strong. Thus, for $Wv\ln(\gamma^2/D^2) \geqslant 1$, formula (68) would give two sharp peaks symmetrically located along the voltage axis near ε_d. This behavior is an artifact of the ladder approximation, although it correctly indicates the presence of an additional peak near the threshold voltage.

As for diagrammatic series of perturbation theory of the type as in this problem, we can improve the ladder approximation by summing up so-called parquet graphs. The fact is that in the presence of a large logarithmic parameter, the ladder diagrams do not belong to the unique class of 'singular' diagrams containing the maximum degree of the logarithm. If one looks at the first diagram in Fig. 16b, it will be seen that a new 'loop' appears from the Green's functions G_kG_d, as the corresponding integral contains a large logarithm at a small 'total energy' $(\omega + \omega_1)$. But a significant integration domain over ω and ω_1 is just a region of low frequencies ω. It is this region that makes a greatest contribution to logarithmic factor L when integrating other pairs of functions $G_{kk}^{<}G_{dd}^{A(R)}$. Thus, the central loop also introduces a logarithmic factor into the overall result.

Our method consists in leaving the most divergent terms proportional to $(Wv)^nL^{n+1}$ in the nth order of perturbation theory, the terms keeping the maximum power of a large logarithm for a given order. Such terms are described by a series of parquet diagrams obtained by successive substitution of two types of loops instead of simple Coulomb vertices, similarly to what was done for constructing two second-order diagrams from the first-order one (see Fig. 16b). Parquet diagrams describe electron scattering in a metal on the impurity Coulomb potential in the two 'most singular' channels. For such a series of diagrams, we can write out approximate integral equations which represent some generalization of the Bethe–Salpeter equation. Integral equations can be solved with a logarithmic accuracy [37, 38].

We face the parquet case 'in its pure form' when occupation numbers for the local level are very small, $n_d \ll 1$ — that is, when $\gamma_p \ll \gamma_k$. In this case, the entire diagram series contains only (++) loops successively inserted into the place of interaction vertices. A combination of Green's functions $G_k^{<}G_d^{R}$, which gives logarithmic factor L (66) upon integrating, is what remains in each such loop. Summation of the parquet series of diagrams leads to the expression [37]

$$J(V) = \gamma_k\,\frac{1 - \exp(-2L)}{2Wv}. \quad (69)$$

The current is determined by the imaginary part of $J(V)$, so that the answer from the leading approximation containing the real part of logarithmic integrals alone is insufficient. From the form of expression (59), it is clear that to all integrals containing the Fermi distribution n_k the imaginary part $i\gamma$ enters additively with energy ε_d. Therefore, the same sum of diagrams will lead with logarithmical accuracy to answer (69) in which $L = Wv\ln X$ $(X = (\varepsilon_d - eV + i\gamma)/D)$.

This result can be generalized for arbitrary values of n_d. The highest contributions with respect to the logarithmic parameter are those that appear in the imaginary part of $J(V)$, when the $G_k^{R}G_d^{<}$ summand is accounted for only in one pair of functions. Moreover, it is easy to see from formulas (62) and (66) that the imaginary part proportional to n_d enters into all expressions in exactly the same way as the imaginary part of the basic logarithmic integral. This allows us, in the first order in the ratio of the imaginary part to the logarithmically large real part, to write out the answer for $\operatorname{Im} J(V)$ from formula (69):

$$I(V) = \operatorname{Im} J(V) = \gamma_k\left[\frac{\partial}{\partial\ln X}\,\frac{1 - \exp(-2L)}{2Wv}\right]\Phi. \quad (70)$$

In this expression, L no longer contains its imaginary part, retaining the real logarithm only [see formula (66)]. Substituting explicit expressions for L and Φ, we obtain the final expression for current:

$$I(V) = \frac{\gamma_k\gamma_p}{\gamma}\left[\frac{D^2}{(eV - \varepsilon_d)^2 + \gamma^2}\right]^{-Wv}$$
$$\times\left[\operatorname{arccot}\left(\frac{\varepsilon_d - eV}{\gamma}\right) - \operatorname{arccot}\left(\frac{\varepsilon_d}{\gamma}\right)\right], \quad (71)$$

where $W < 0$. The parquet approximation is more accurate than the ladder one, allowing us to describe the behavior of the current–voltage characteristics near the threshold. We note, however, that if one takes into account the imaginary parts of the Green's function, which is necessary for tunnel problems, the restriction in the perturbative series by the parquet diagrams is an approximation since, strictly speaking, we disregard a series of diagrams that have the same order of magnitude in powers of $\ln|X|$. Nevertheless, both the ladder approximation and the parquet diagram series unequivocally indicate the appearance of a peak in the current–voltage characteristics, which is associated with Coulomb correlation effects. Formula (71) allows us to estimate the value of an additional peak and general behavior of the tunnel characteristics.

In addition to the case considered, when the tunneling of electrons from the impurity level creates a positively charged hole, it is also feasible that, for a different voltage polarity, the electron after tunneling will occupy the impurity state, creating an additional repulsive potential for electrons in the metal. In this case, formula (71) also defines the tunneling current, but the sign of Coulomb interaction should be changed to the opposite one: $W > 0$. Coulomb correlations lead to current suppression near the threshold, while its dependence on voltage has a power-law character.

Examples of tunnel characteristics calculated for these two possible cases are given in Fig. 17.

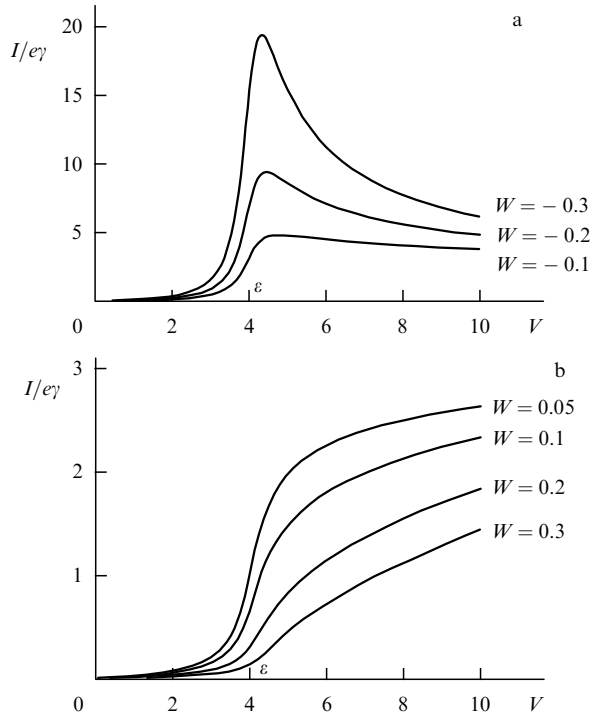

Figure 17. Current–voltage curve for various values of Coulomb interaction. The current is plotted in dimensionless units $I/e\gamma$. (a) $w = Wv < 0$, $\varepsilon_d = 0.4$ eV, and (b) $w = Wv > 0$, $\varepsilon_d + U = 0.4$ eV, $\gamma_t/\gamma = 3$, $\varepsilon_d/\gamma = 40$.

We note that in Ref. [39] the correct assumption on the possible appearance of such a singularity was put forward. However, an attempt to apply the language of penetration coefficients found for the equilibrium case has led to a completely incorrect formula for the current at arbitrary γ_k and γ_p. Another wrong conclusion concerns the use of the parquet approximation for a completely filled level, $n_d \simeq 1$, while the analysis of the nonequilibrium situation shows that a simple parquet series is reproduced in the opposite limit of $n_d \ll 1$. The possibility of the existence of suppressed conductivity near the threshold at a different voltage polarity has also been missed.

An experimental study of a GaAs surface doped with Mn atoms [33] revealed that tunnel characteristics measured at the impurity location point differ significantly from those over the rest of the surface and correspond to the behavior described by formula (71).

Results of calculations are displayed in Fig. 17. Its main feature is that the tunneling conductivity itself near the impurity atom is suppressed at positive voltages of 0.5–1.5 V, while the normalized differential conductivity has a peak. It is this unusual behavior that formula (71) describes for a positive sign of Coulomb interaction.

A singular behavior of the current–voltage characteristics can arise when two coupled quantum dots undergo tunneling through a system in the presence of Coulomb interaction of charges localized at various points. In this case, thanks to the interaction of localized electrons with a continuous spectrum in the contact leads, the electron energy levels in quantum dots acquire a finite width. The behavior of current–voltage characteristics when the voltage across the contact is varied might be described by formulas analogous to Eqn (71), provided the tunneling level width γ plays the role of the band width v^{-1}.

8. Conclusion

In this review, we described experimental data obtained using scanning tunneling microscopy/spectroscopy, which most clearly manifest an influence of nonequilibrium tunneling effects and electron spectrum reconstruction. We also propose a theoretical explanation based on the self-consistent consideration of the nonequilibrium distribution of electrons and the change in the electron density of states in the tunneling contact area with flowing tunneling current. The theory explains the appearance of induced tunneling conductivity in low-dimensional and nanoscale structures which results from the emergence of bound states in the band gap and at a finite relaxation rate of nonequilibrium electrons.

The presented theoretical approach makes it possible to understand the causes of the anomalous band gap width experimentally observed in semiconductors, resulting from the appearance of nonequilibrium charges in the tunnel junction region. Our theoretical analysis explains the appearance of tunneling conductivity peaks near boundaries of the semiconductor band gap, whose position depends on the geometry of the experiment and weakly varies upon changing the initial impurity level energies. The peaks in tunneling conductivity appearing in a semiconductor band gap are accompanied by a decrease in the density of states in the allowed spectrum region, as opposed to its unperturbed value. A theoretical analysis of nonequilibrium interference effects driven by tunneling through interacting impurity atoms in the Anderson model has been experimentally confirmed by STS studies of interacting impurities on the surface of semiconductors.

An experimental study of impurity atoms on a semiconductor surface with deep energy levels by scanning tunneling microscopy/spectroscopy methods revealed a nonmonotonic dependence of tunneling current on the voltage across the tunnel junction. According to the proposed theoretical model, this behavior can be explained by the formation of singularities in current–voltage characteristics, caused by the renormalization of the tunneling amplitudes driven by the exciton type Coulomb interaction for certain kinds of impurity atoms.

This study was supported by the Russian Science Foundation under the grant 16-12-00072.

References

1. Binning G et al. *Phys. Rev. Lett.* **50** 120 (1983)
2. Marczinowski F et al. *Phys. Rev. Lett.* **99** 157202 (2007)
3. Feenstra R M *Phys. Rev. Lett.* **63** 1412 (1989)
4. Madhavan V et al. *Phys. Rev. B* **64** 165412 (2001)
5. Morgenstern M et al. *Phys. Status Solidi B* **210** 845 (1998)
6. Mahieu G et al. *Phys. Rev. Lett.* **94** 026407 (2005)
7. Sullivan J M et al. *Phys. Rev. B* **68** 235324 (2003)
8. Wolf E L *Principles of Electron Tunneling Spectroscopy* (New York: Oxford Univ. Press, 1985); Translated into Russian: *Printsipy Elektronnoi Tunnel'noi Spektroskopii* (Kiev: Naukova Dumka, 1990)
9. Maslova N S et al. *JETP Lett.* **67** 146 (1998); *Pis'ma Zh. Eksp. Teor. Fiz.* **67** 130 (1998)
10. Maslova N S et al. *Phys. Status Solidi A* **131** 35 (1992)
11. Maslova N S et al. *Solid State Commun.* **95** 507 (1995)
12. Zheng J F et al. *Phys. Rev. Lett.* **72** 1490 (1994)
13. Depuydt A et al. *Phys. Rev. B* **60** 2619 (1999)
14. Maslova N S, Panov V I, Savinov S V *Phys. Usp.* **43** 531 (2000); *Usp. Fiz. Nauk* **170** 575 (2000)
15. Marczinowski F et al. *Phys. Rev. B* **77** 115318 (2008)

16. Depuydt A et al. *Appl. Phys. A* **66** S171 (1998)
17. Arseev P I, Maslova N S, Panov V I, Savinov S V *JETP* **94** 191 (2002); *Zh. Eksp. Teor. Fiz.* **121** 225 (2002)
18. Anderson P W *Phys. Rev.* **124** 41 (1961)
19. Mahan G D *Phys. Rev.* **163** 612 (1967)
20. Matveev K A, Larkin A I *Phys. Rev. B* **46** 15337 (1992)
21. Arseyev P I, Maslova N S, Panov V I, Savinov S V *JETP Lett.* **76** 287 (2002); *Pis'ma Zh. Eksp. Teor. Fiz.* **76** 345 (2002)
22. Keldysh L V *Sov. Phys. JETP* **20** 1018 (1965); *Zh. Eksp. Teor. Fiz.* **47** 1515 (1964)
23. Arseev P I *Phys. Usp.* **58** 1159 (2015); *Usp. Fiz. Nauk* **185** 1271 (2015)
24. Arseyev P I, Volkov B A *Solid State Commun.* **78** 373 (1991)
25. Arseev P I, Maslova N S *JETP* **75** 575 (1992); *Zh. Eksp. Teor. Fiz.* **102** 1056 (1992)
26. Arseev P I, Maslova N S, Mantsevich V N *JETP* **115** 141 (2012); *Zh. Eksp. Teor. Fiz.* **142** 156 (2012)
27. Maslova N S, Arseyev P I, Mantsevich V N *Solid State Commun.* **241** 20 (2016)
28. Bardeen J *Phys. Rev. Lett.* **6** 57 (1961)
29. Feenstra R M, Fein A P *Phys. Rev. B* **32** 1394(R) (1985)
30. Zheng Z F, Salmeron M B, Weber E R *Appl. Phys. Lett.* **64** 1836 (1994)
31. Lengel G et al. *J. Vac. Sci. Technol. B* **11** 1472 (1993)
32. Renner Ch, Fischer O *Phys. Rev. B* **51** 9208 (1995)
33. Arseyev P I, Maslova N S *Solid State Commun.* **108** 717 (1998)
34. Domke C et al. *J. Vac. Sci. Technol. B* **16** 2825 (1998)
35. Pacherová O et al. *Czech. J. Phys.* **49** 1621 (1999)
36. Arseev P I et al. *JETP Lett.* **72** 565 (2000); *Pis'ma Zh. Eksp. Teor. Fiz.* **72** 819 (2000)
37. Arseyev P I, Maslova N S, Savinov S V *JETP Lett.* **68** 320 (1998); *Pis'ma Zh. Eksp. Teor. Fiz.* **68** 299 (1998)
38. Beenakker C W J *Phys. Rev. B* **44** 1646 (1991)
39. Kaminski A, Glazman L I *Phys. Rev. B* **61** 15927 (2000)